AD-A249 726

UMENTATION PAGE

Form Approved
OMB No 0704-0188

2. REPORT DATE	3. REPORT TYPE AND DATES COVERED
1991	THESIS/DISSERTATION

4. TITLE AND SUBTITLE
Precipitation Distribution and Kinematic Structure of
Hurricane Hugo Over the Carolinas

5. FUNDING NUMBERS

6. AUTHOR(S)

James E. Hammett, Jr., Capt

7. PERFORMING ORGANIZATION NAME(S) AND ADDRESS(ES)

AFIT Student Attending: North Carolina State University

8. PERFORMING ORGANIZATION REPORT NUMBER

AFIT/CI/CIA- 91-113

9. SPONSORING/MONITORING AGENCY NAME(S) AND ADDRESS(ES)

AFIT/CI
Wright-Patterson AFB OH 45433-6583

DTIC
ELECTE
MAY 6 1992
S C D

10. SPONSORING/MONITORING AGENCY REPORT NUMBER

11. SUPPLEMENTARY NOTES

12a. DISTRIBUTION/AVAILABILITY STATEMENT
Approved for Public Release IAW 190-1
Distributed Unlimited
ERNEST A. HAYGOOD, Captain, USAF
Executive Officer

12b. DISTRIBUTION CODE

13. ABSTRACT (Maximum 200 words)

14. SUBJECT TERMS

15. NUMBER OF PAGES
47

16. PRICE CODE

17. SECURITY CLASSIFICATION OF REPORT	18. SECURITY CLASSIFICATION OF THIS PAGE	19. SECURITY CLASSIFICATION OF ABSTRACT	20. LIMITATION OF ABSTRACT

ABSTRACT

HAMMETT, JAMES E. JR. Precipitation Distribution and Kinematic Structure of Hurricane Hugo over the Carolinas. (Under the direction of Steven Businger and Gerald F. Watson.)

An investigation of the precipitation distribution and kinematic structure of Hurricane Hugo over land was conducted for a 19-hour period beginning with landfall of associated precipitation. Surface kinematics and thermodynamics, NWS radar reflectivity observations, and hourly precipitation data (HPD) were compared to investigate the nature of the precipitation systems associated with Hugo. Surface data over Georgia, South Carolina, North Carolina, and Virginia from the NWS, AWS, and FAA stations was supplemented by power plant data.

A stationary band complex (SBC), observed to the left of Hugo's track, was the predominate feature of radar imagery. This feature resulted in a storm-total rainfall maximum to the left of Hugo's track. Heavy amounts of hourly rainfall (> 20 mm) occurred within the SBC from 0500 UTC until 1000 UTC, and an equivalent potential temperature minima is associated with the SBC after landfall of Hugo.

A regression equation was constructed to investigate the hourly precipitation for select land stations. The results indicate that over 37% of the variability in the HPD was accounted for when precipitation was occurring during Hugo. The distance to the eyewall contributed significantly to the variability of precipitation over land, in this case. It was found that terrain slope, surface wind speed, surface wind direction, and surface wind convergence were generally uncorrelated to hourly precipitation. However, when the data set was separated into geographic regions, terrain slope increased in importance from the coast to the mountains while wind speed decreased in importance.

92-11983

92- 5 01 021

PRECIPITATION DISTRIBUTION
AND KINEMATIC STRUCTURE
OF HURRICANE HUGO OVER THE CAROLINAS

by

JAMES EDWARD HAMMETT, JUNIOR

A thesis submitted to the Graduate Faculty of
North Carolina State University
in partial fulfillment of the
requirements for the Degree of
Master of Science

DEPARTMENT OF MARINE, EARTH, AND ATMOSPHERIC SCIENCE

Raleigh

1991

APPROVED BY:

STEVEN BUSINGER
Co-chairman

GERALD F. WATSON
Co-chairman

D. W. NYCHKA

ACKNOWLEDGEMENTS

TABLE OF CONTENTS

LIST OF TABLES

LIST OF FIGURES

LIST OF SYMBOLS AND ABBREVIATIONS

ANOVA	Analysis of Variance
AWS	Air Weather Service
b_i	Regression coefficient estimate
B_i	Model coefficient estimate
$^\circ C$	Degrees Centigrade
CON	Convergence
cos	Cosine
D	Dimensional
Dep Mean	The overall average of the variable
DEW	Distance to the eyewall
Exp	Exponent
F Value	Model sum of squares divided by the model mean square
FAA	Federal Aviation Administration
h	Hour
HPD	Hourly precipitation data
K	Kelvin temperature
km	Kilometers
log	Natural logarithm
mb	Millibars
mm	Millimeters
$m\ s^{-1}$	Meters per second
NCDC	National Climatic Data Center
NWS	National Weather Service

p-value	Test for significance
Prob	Probability
Q	Mean of any meteorological variable
Q_i	Observed value of any meteorological variable at a grid point
r	Radius
R^2	Model sum of squares divided by the total sum of squares
Root MSE	Square root of the mean square for error
SA	Surface observations
SBC	Stationary band complex
Sept	September
SN	Slope number
T for HO	T-value for testing the null hypothesis that the parameter equals 0
t-value	Test for Significance
tan	Tangent
UTC	Universal time code
VIP level	Reflectivity intensity level
WD	Wind direction
w_i	Observational weight given to a meteorological variable
WS	Wind speed
y(obs)	Observation point for the regression equation
Y(obs)	Observation point for the model
α	smoothing parameter
>	greater than
<	less than
%	percent

1. INTRODUCTION

Hurricane Hugo was the strongest storm to hit the continental United States in twenty years (since Hurricane Camille of 1969), but it caused much more damage than Camille. Sheets (1990) estimated the total property loss from Hugo to be more than 7 billion dollars in the continental United States, compared to less than 1.5 billion for Camille (Simpson et al., 1970). Case and Mayfield (1990) estimated there were 49 deaths associated with Hurricane Hugo. South Carolina's 13 casualties made it the hardest hit state.

The organized convective rainfall and strong winds of Hugo produced widespread flooding, significant property damage, and considerable human suffering. Other hurricanes have caused only minor damage after landfall. This large variation in flooding, human suffering, and property damage emphasize the need for improved understanding of rainfall and wind patterns as these powerful tropical cyclones enter the eastern United States.

Tropical storm rainfall was first examined by Cline (1926) through analysis of raingauge data from states bordering the Gulf of Mexico during the landfall of eight storms. The author found that a rainfall maximum tended to occur in the right front quadrant relative to the storm motion. Cline's results were supported by Koteswaram and Gasper (1956), who examined four cyclones on the east coast of India. Miller (1958) analyzed hourly raingauge reports from 16 hurricanes that affected Florida. He found a slight bias in rainfall to the right of the track, but concluded the difference between sides of the storm was insignificant. Dunn and Miller (1960) hypothesized that increased surface friction during landfall enhances low-level convergence and accounts for higher rain rates to the right of the storm track at the coastline.

Parrish *et al.* (1982) examined digitized radar data during the landfall of Hurricane Frederic (1979). They found that 50 km inland from the coast the rain totals near the storm track decreased by a factor of two. Areas with the greatest wind damage tended to occur in regions with the highest rainfall rates.

Willoughby *et al.* (1984) identified the stationary band complex (SBC) as a prominent spiral band in tropical cyclones that maintains a fixed position relative to the vortex. The SBC moves slowly, if at all, and its tangential wavenumber is approximately one. The SBC was defined by cellular convective precipitation returns on radar. Between the SBC and eyewall stratiform rainfall occurred. Equivalent potential temperatures generally increased from the SBC to the eyewall.

A composite study of the surface wind field of hurricane Donna, which occurred in 1960, by Miller (1963, 1964) was first to indicate that the main reason for weakening of a tropical storm after landfall was the loss of its latent heat source. Bradbury (1971) studied changes in radar echo motion and the surface pressure field for two 9-h periods before and after the landfall of Hurricane Camille in 1969 in another composite study. She found the maximum winds or echo motion for Camille switched from the right forward sector before landfall to the right rear quadrant after landfall.

Moss and Jones (1978) suggested frictional and thermal effects over land may influence the future motion of the storm. Later, while examining the low-level wind structure of hurricane Frederic (1979), Powell (1982) hypothesized that frictional and thermal effects over land may produce features in the mesoscale wind and precipitation structure that are related to the areas of heaviest damage.

The Hurricane Strike program at the National Hurricane Research Laboratory (NHRL) established in 1956 in Miami, Florida is the most important source of data for constructing the three-dimensional structure of the tropical cyclone. Their specially

equipped aircraft have flown more than 400 missions at various altitudes into hurricanes and tropical storms, investigating physical changes in the behavior of tropical cyclones as they approach land. Their collection and interpretation of data for hurricanes; Frederick (1979), Alicia (1983), and Hugo (1989), by Powell have provided significant insights into the physical changes of storms during the landfall process.

Powell's (1987) post-landfall analysis of Hurricane Alicia (1983) identified a stationary band complex (SBC) to the northeast of the storm center associated with an outer rainband region. The rainband axis was associated with strong surface convergence while the area between the axis and the eyewall displayed surface divergence.

Numerical models by Myers and Malkin (1961) and Chow (1971) were constructed to depict the surface wind field from the observed characteristics of storms. *More sophisticated 3-D numerical models by Moss and Jones (1978) and Tuleya et al.* (1984) have recently been employed to study the effects of landfall on a storm. The aim of Tuleya et al's nested-mesh model was to attempt to isolate decay mechanisms of hurricanes over land. A hurricane was spun-up over water by the model, then tracked toward the coast with a base flow of 10 m s^{-1}. The authors found that two hours after landfall, the area of heavy precipitation (> 28.8 mm h^{-1}) decreased as the storm decayed. The experiment was repeated with a roughness field which varied from 10 cm at the coast to 100 cm 1.5 degrees of latitude inland. The 10 cm roughness field was representative of grasslands along the coast and the 100 cm field represented trees further inland. A small increase of surface central pressure occurred while the storm was over the 100 cm area, but there were no large differences in the storm total rainfall amounts. This result suggests that terrain slope and frictional effects on rainfall amount may be minimal.

History of Hugo

The precursor to Hurricane Hugo was detected on 9 September 1989 by satellite imagery when a cluster of thunderstorms moved off the coast of Africa. The official best track begins on 10 September when a tropical depression formed to the southeast of the Cape Verde Islands. Moving westward at 9 m s^{-1} across the tropical Atlantic Ocean, Hugo became a tropical storm on 11 September and a hurricane on 13 September about 1100 nautical miles east of the Leeward Islands (Fig. 1).

Hugo turned toward the west-northwest and slowed its forward speed as it headed for the Leeward Islands in response to low pressure at 500 mb north of Puerto Rico which represented a weakness in the subtropical high pressure ridge. Hugo's eye passed over Guadeloupe Island at 0500 UTC on 17 September with 62 m s^{-1} winds, and then crossed the island of St Croix one day later.

Hugo was centered just a few hundred miles east of Florida by 21 September. Final landfall was made at Sullivans Island on the South Carolina coast at 0400 UTC on 22 September, with the eye moving northwestward at 12 m s^{-1}. The National Weather Service office at the Charleston airport measured steady winds of 35 m s^{-1} with gusts to 44 m s^{-1}. A report of a gust to 48 m s^{-1} was observed at downtown Charleston.

Maintaining hurricane strength but gradually weakening, Hugo's eye passed between Columbia and Shaw Air Force Base around 0800 UTC. Shaw Air Force Base reported steady winds of 30 m s^{-1} with a gust to 49 m s^{-1}. Hugo was still a relatively strong storm as far inland as North Carolina. Even though Hugo was downgraded to a tropical storm by 1200 UTC, steady winds of 31 m s^{-1} with gusts to 44 m s^{-1} were reported at Charlotte, North Carolina.

Hurricane Hugo
"Best Fit" Track

0000 13 Sept 89
0000 14 Sept 89
0000 15 Sept 89
0000 16 Sept 89
0000 17 Sept 89
0000 18 Sept 89
0000 19 Sept 89
0000 20 Sept 89
0000 21 Sept 89
0000 22 Sept 89
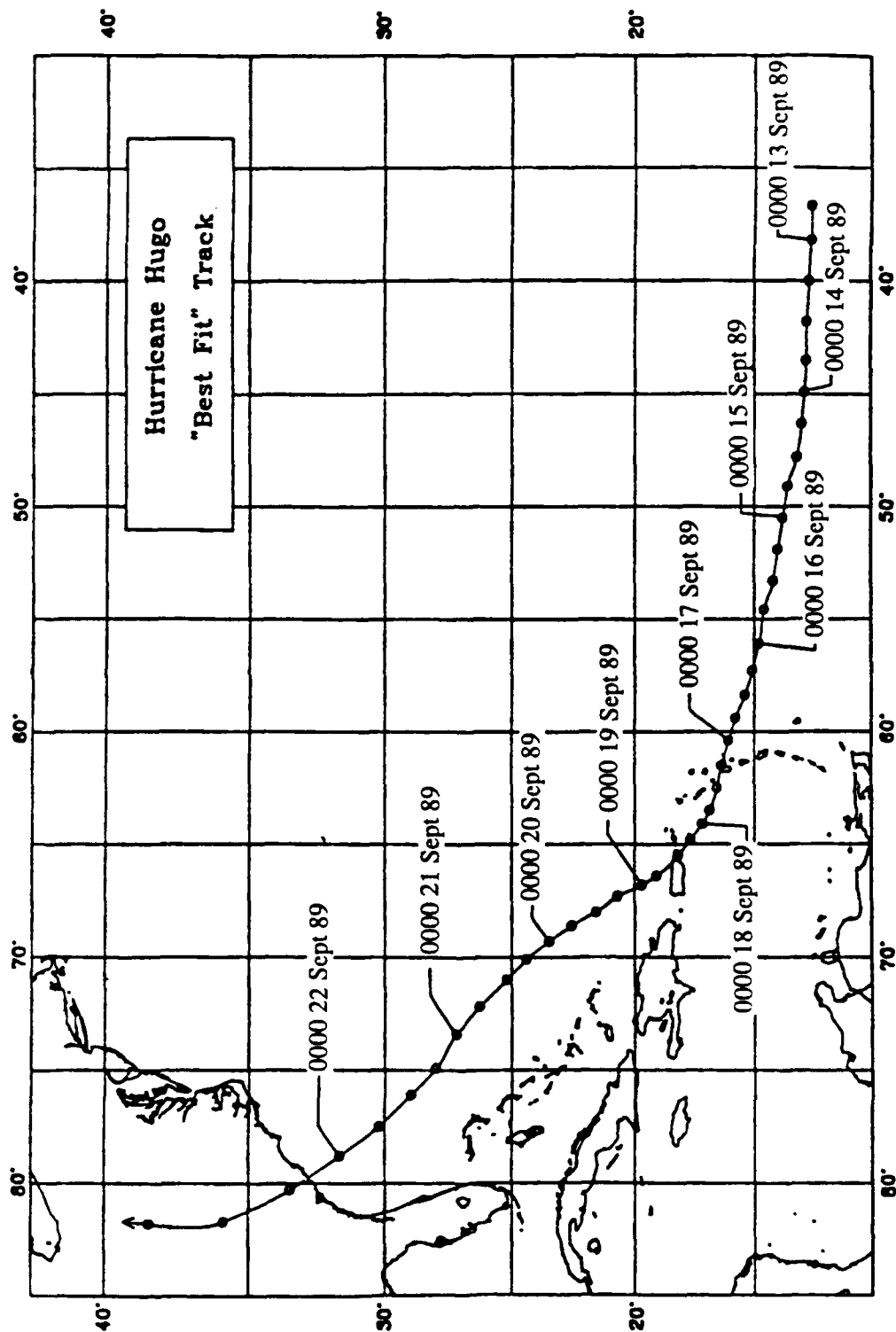
1. Hurricane Hugo's storm track.

The storm's unusual track through the Carolina's was the result of a 500 mb high pressure system off the coast of New England and a pronounced low aloft over the Gulf of Mexico (Fig. 2). These two systems forced Hugo to the northwest until a major longwave trough in the central U.S. gradually turned Hugo to the north (Fig. 3).

As the major longwave trough approached the Appalachian Mountains, strong south-southwesterly flow forced Hugo northward across western Virginia, West Virginia, eastern Ohio, and western Pennsylvania. Hugo transformed into an extratropical disturbance near Lake Erie by 0000 UTC on 23 September. The storm was tracked for two more days as it moved northeastward across eastern Canada and into the far north Atlantic Ocean.

The objectives of the present research are to:

i) Document the structure and evolution of the stationary band complex (SBC) and eyewall of Hurricane Hugo through examination of the hourly precipitation data (HPD) and radar reflectivity data over land.

ii) Investigate relationships between surface wind convergence, pressure, equivalent potential temperature, and the hourly rainfall distribution within the eyewall and stationary band complex (SBC) over the Carolinas.

iii) Develop a multiple regression equation to predict hourly precipitation for Hugo over land, then partition the data set into geographic regions to further examine the significance of the independent variables.

500 mb Analysis
1200 UTC 21 Sept 1989
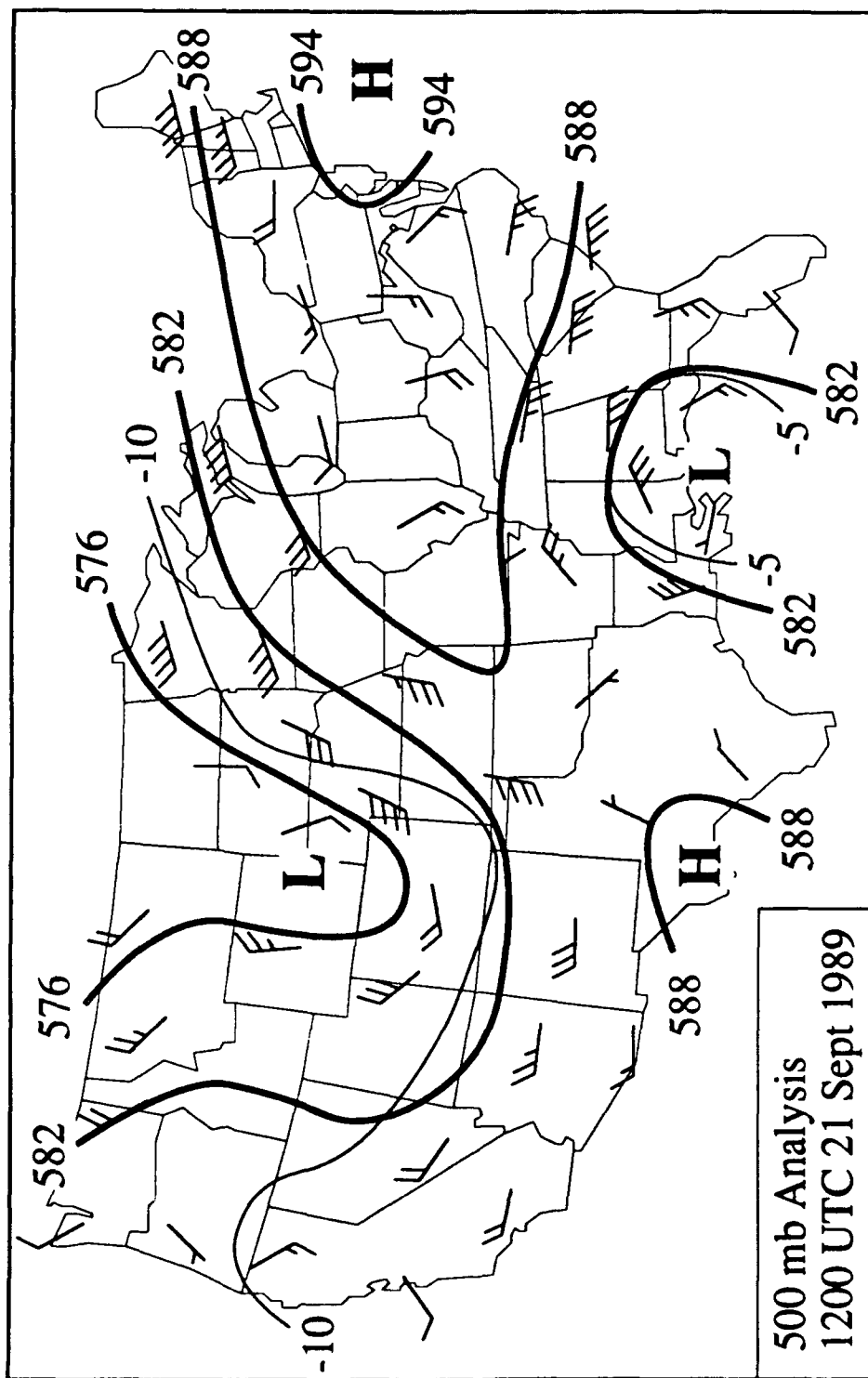
2. 500 mb analysis at 1200 UTC on 21 September 1989. Height contours (thick lines) in decameters. Thin lines are temperature contours (°C).

500 mb Analysis
1200 UTC 22 Sept 1989
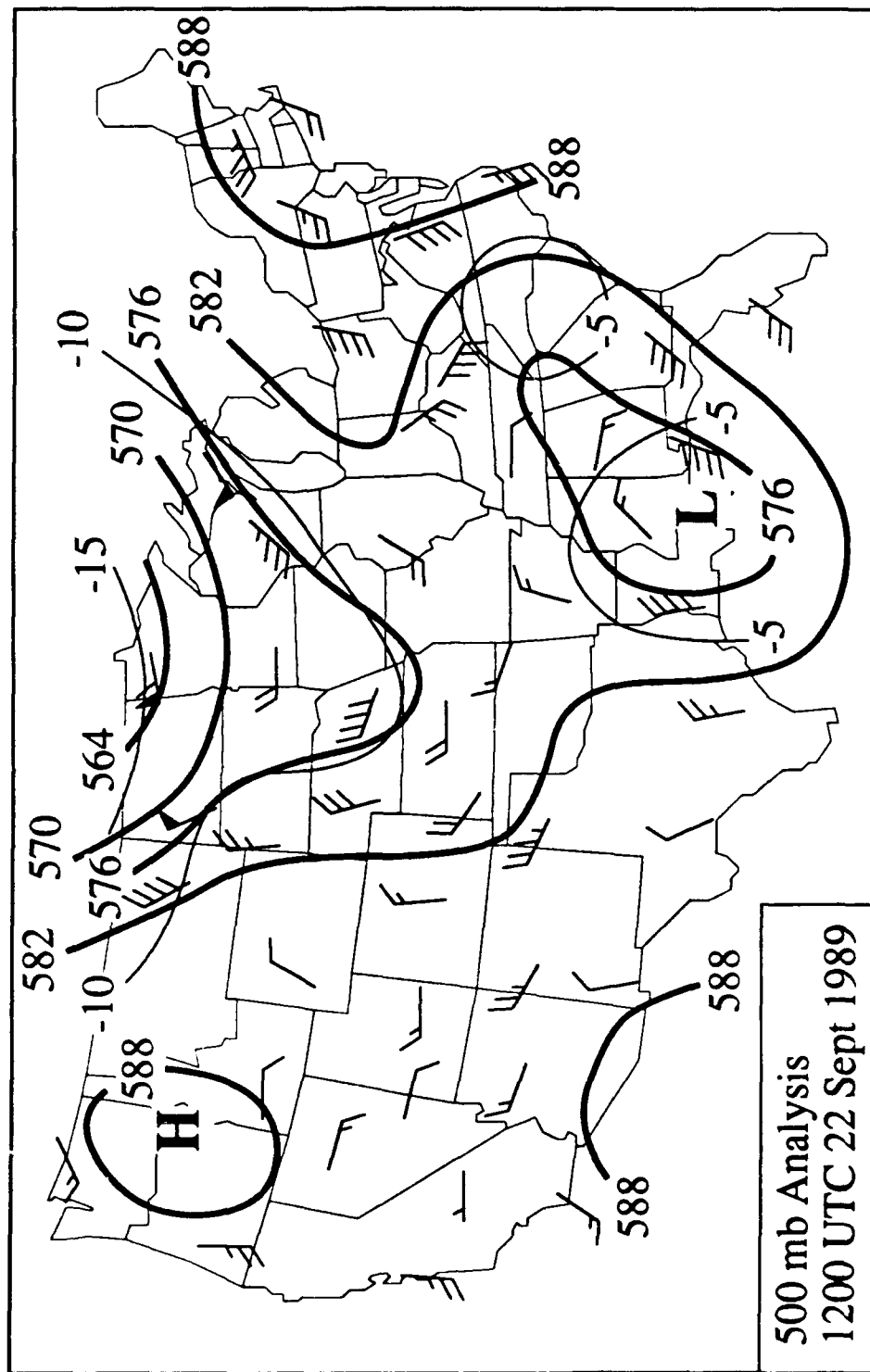
3. 500 mb analysis at 1200 UTC on 22 September 1989. Height contours (thick lines) in decameters. Thin lines are temperature contours (°C).

2. DATA ANALYSIS

Composite radar reflectivity data from the WSI Corporation were examined from 21 September 1989 at 2030 UTC to 22 September at 2330. Each reflectivity image was a composite of all the radars in the area with six levels of reflectivity, but there were no observations above VIP level-3 (Table 1). Hourly precipitation data (HPD) (Fig. 4) and hourly surface observations (SA) (Fig. 5) were obtained from the National Climatic Data Center, as well as all available power plants, for the period 21 September 1989 at 1900 UTC until 22 September at 1300 UTC for Georgia, South Carolina, North Carolina, and Virginia. A single pass Barnes scheme available in UNIDATA WXP software was used to objectively contour (NCAR Graphics) surface wind convergence. The observation weights (w_i) for the stations were defined by: $w_i = \exp(-r^2 / \alpha)$ where r is the distance from the data station to the gridpoint, and α ($\sim$ 1) is the smoothing parameter. Here $0 \leq \alpha \leq 1$ is in normalized, non-dimensional units. The objectively determined value at a gridpoint is just the weighted mean of surrounding observations.

Table 1. Reflectivity Intensity (Federal Meteorological Handbook No. 7A, 1987)

D/VIP Level	Echo Intensity	Estimated Precipitation	Rainfall Rate (mm h^{-1}) Convective
1	Weak	Light	< 5.1
2	Moderate	Moderate	5.1 - 27.9
3	Strong	Heavy	27.9 - 54.9

High pressure is prevalent in northern Virginia at 2100 UTC on 21 September 1989 (Fig. 6a), while the lowest pressures occur along the Georgia/South Carolina coast. An equivalent potential temperature maxima (area > 348 K) covering eastern South Carolina is in close proximity to lowest pressures. Weak surface convergence is
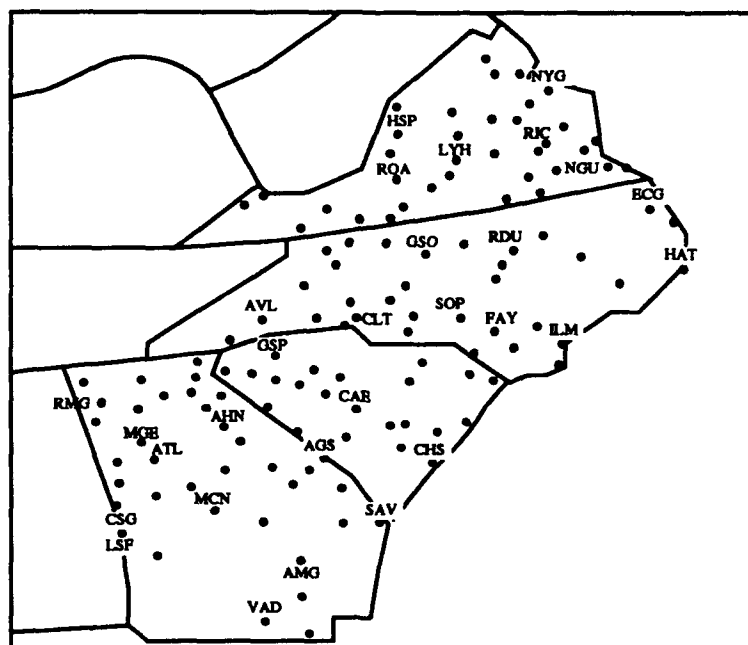
4. Regional area showing locations of NWS and power plant sites that reported hourly precipitation data.
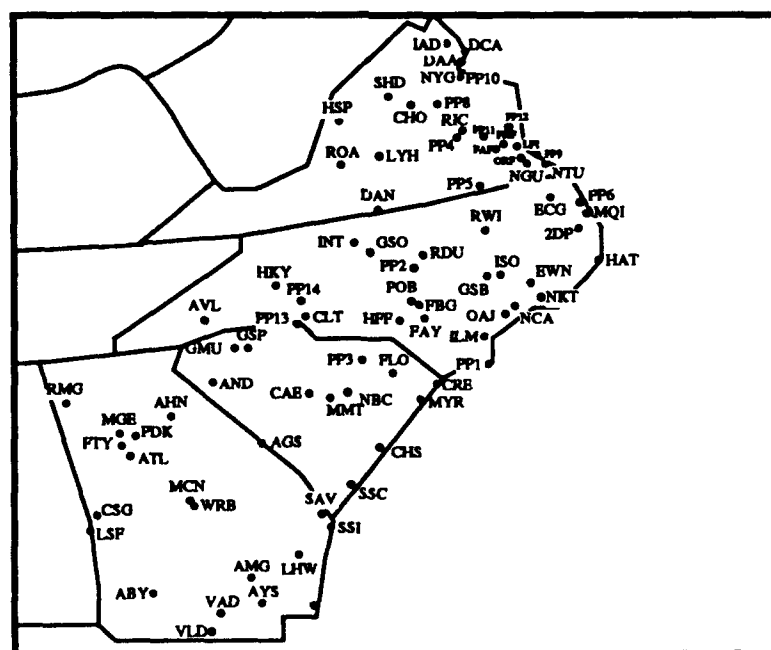
5. Regional area showing locations of NWS and power plant sites that reported hourly surface observations.
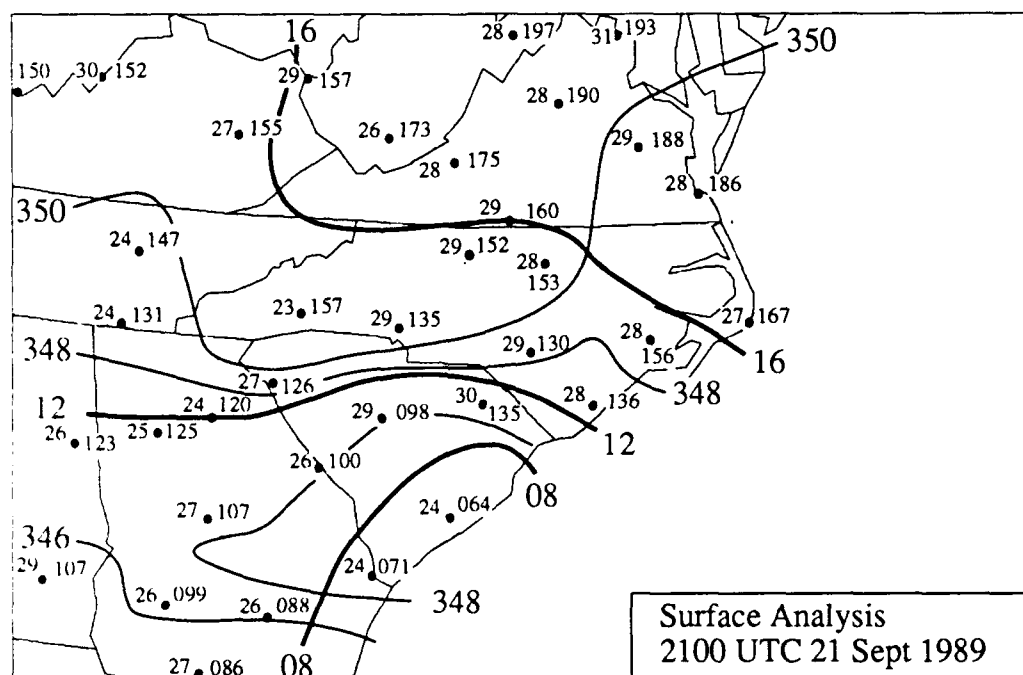
6. a) Surface analysis with sea level pressure (mb) (thick lines) and equivalent potential temperature (K) (thin lines) at 2100 UTC on 21 September 1989.
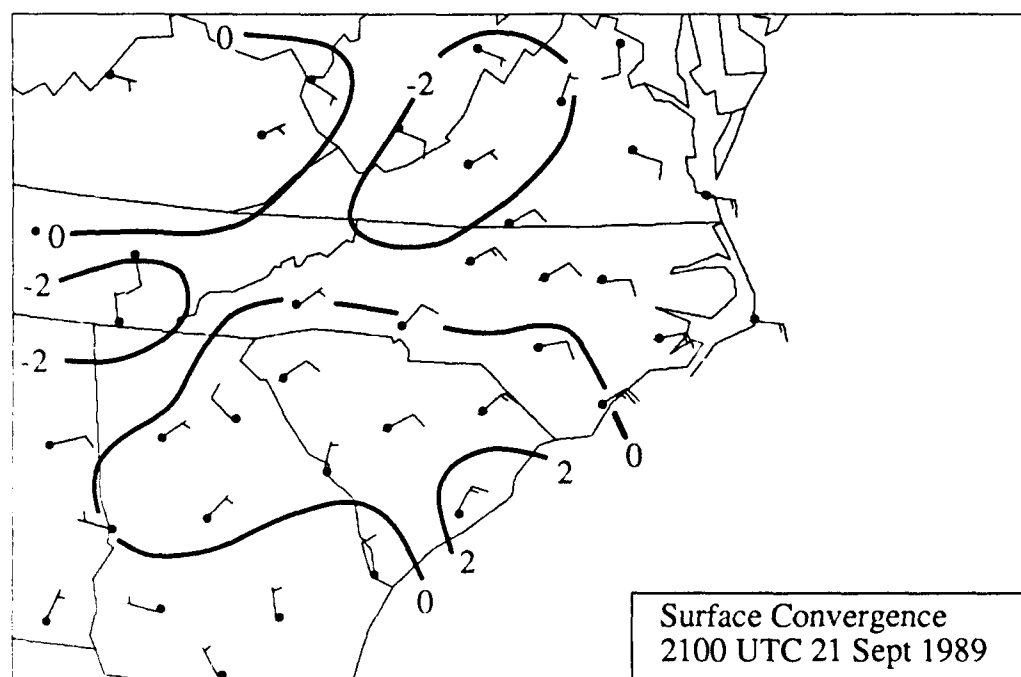
6. b) Surface analysis with wind convergence (10^{-5} s^{-1}) at 2100 UTC on 21 September 1989.
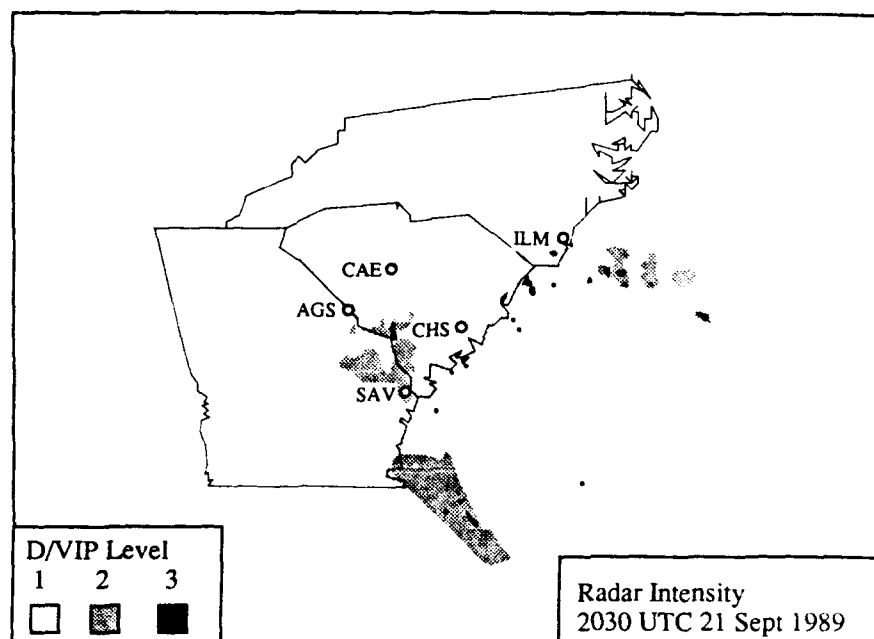
6. c) Composite radar summary with D/VIP levels shaded at 2030 UTC on
21 September 1989.
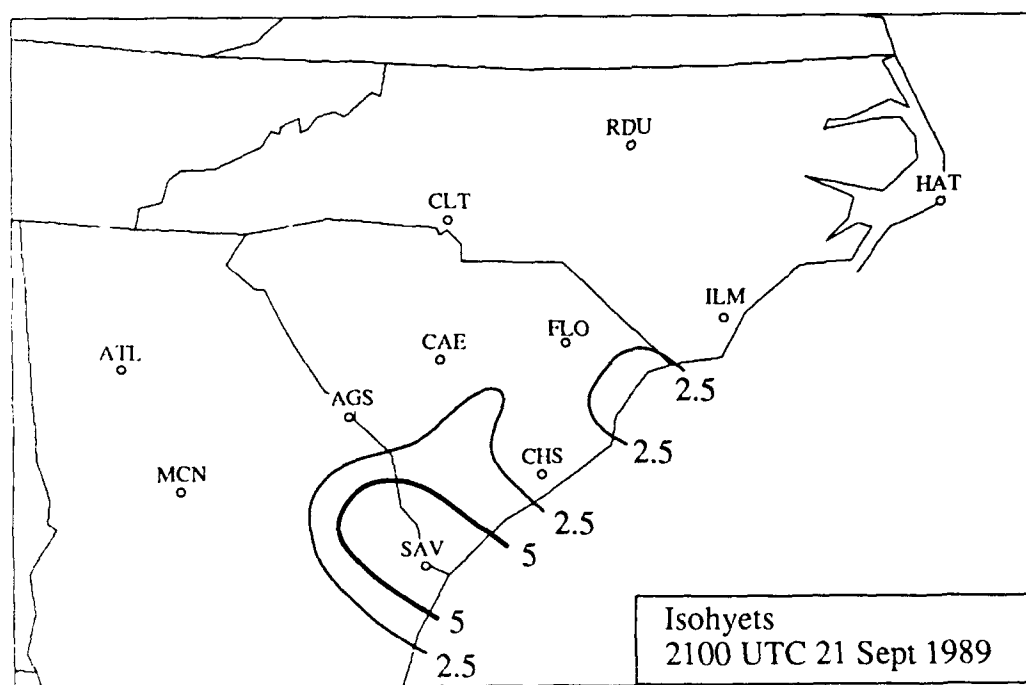
6. d) Analysis of the hourly precipitation data (mm) from 2001 - 2100 UTC
on 21 September 1989.

occurring over most of South Carolina (Fig. 6b), while divergence is observed over most of Virginia, North Carolina, and southern Georgia. Radar reflectivity for 2030 UTC (Fig. 6c) shows a large area of weak (VIP level-1) reflectivity over the Atlantic Ocean extending into southern North Carolina, South Carolina, and Georgia. Two bands of VIP level-2 reflectivity are observed; one off the coast of southern North Carolina and another left of Hugo's eye primarily over the water and running along the South Carolina/Georgia border. This feature to the left of the vortex is a stationary band complex (SBC) as described by Willoughby *et al.* (1984) since the spiral band maintained a fixed position relative to the vortex. An area with rainfall > 5 mm is observed in association with the SBC in the hourly precipitation reported at 2100 UTC (Fig. 6d).

More strongly curved surface isobars enter South Carolina by 22 September at 0000 UTC (Fig. 7a), and the pressure falls below 1000 mb along the coast. Stronger convergence begins its push inland here (Fig. 7b). The 2330 UTC radar reflectivity (Fig. 7c) shows a well-defined eye and eyewall return, with the area of weak reflectivity moving deeper into South Carolina. The SBC has increased in size while maintaining a break in moderate reflectivity near the Georgia coast. The area of precipitation > 5 mm has expanded into South Carolina (Fig. 7d).

The pressure and equivalent potential temperature gradients over South Carolina at 0300 UTC (Fig. 8a) tighten significantly as pressure continues to fall and equivalent potential temperatures rise. A strong convergent area > 8×10^{-5} s^{-1} (Fig. 8b) appears along the front left side of Hugo, while pockets of divergence occur over Georgia, North Carolina, and Virginia. The area of weak echo returns continues a northwestward movement at 0230 UTC (Fig. 8c), while the SBC maintains its predominate size and shape. The VIP level-2 band off the North Carolina coast at 2030 UTC is no longer
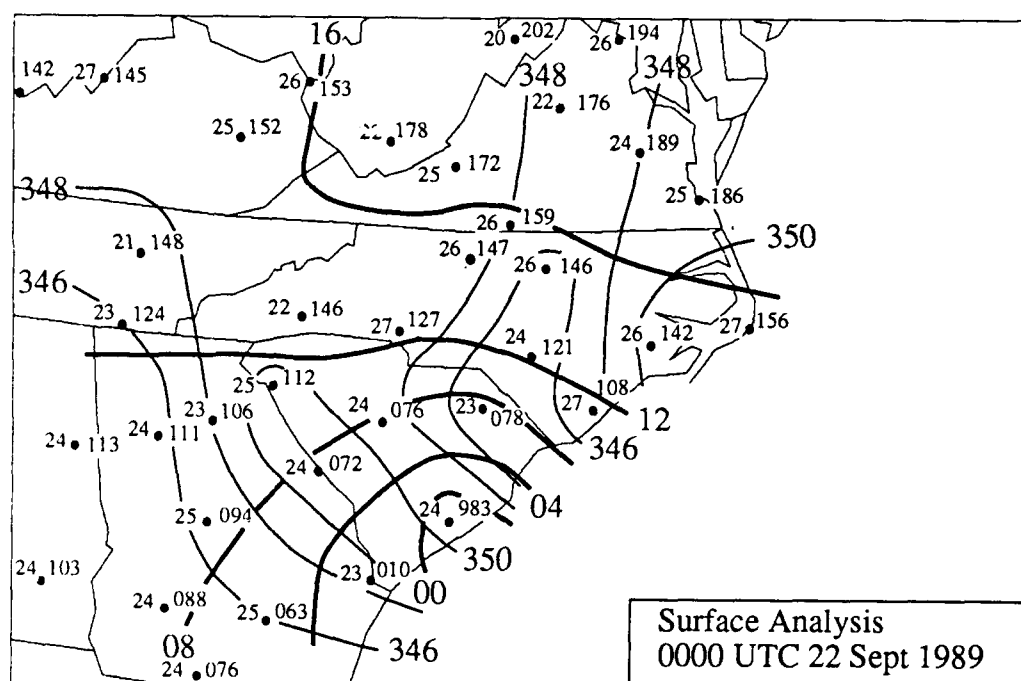
7. a) Surface analysis with sea level pressure (mb) (thick lines) and equivalent potential temperature (K) (thin lines) at 0000 UTC on 22 September 1989.

7. b) Surface analysis with wind convergence (10^{-5} s^{-1}) at 0000 UTC on 22 September 1989. Large black dot represents Hugo's eye.
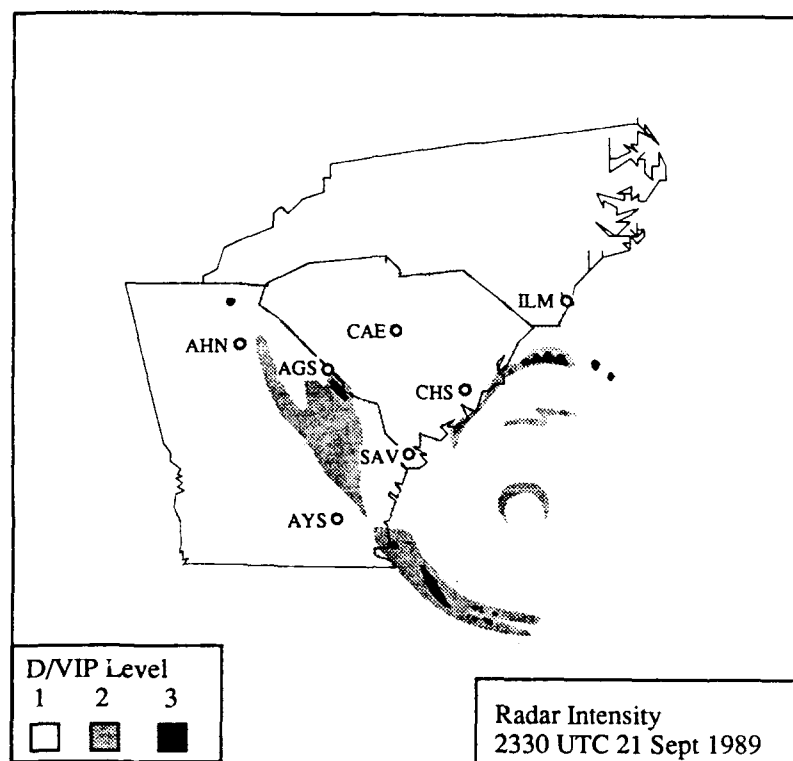
7. c) Composite radar summary with D/VIP levels shaded at 2330 UTC on
21 September 1989.

7. d) Analysis of the hourly precipitation data (mm) from 2301 - 0000 UTC
on 22 September 1989. Large black dot represents Hugo's eye.

8. a) Surface analysis with sea level pressure (mb) (thick lines) and equivalent potential temperature (K) (thin lines) at 0300 UTC on 22 September 1989. Note that isobars are analyzed at 8 mb increments near the eye.

8. b) Surface analysis with wind convergence (10^{-5} s^{-1}) at 0300 UTC on 22 September 1989. Large black dot represents Hugo's eye.

8. c) Composite radar summary with D/VIP levels shaded at 0230 UTC on
22 September 1989.
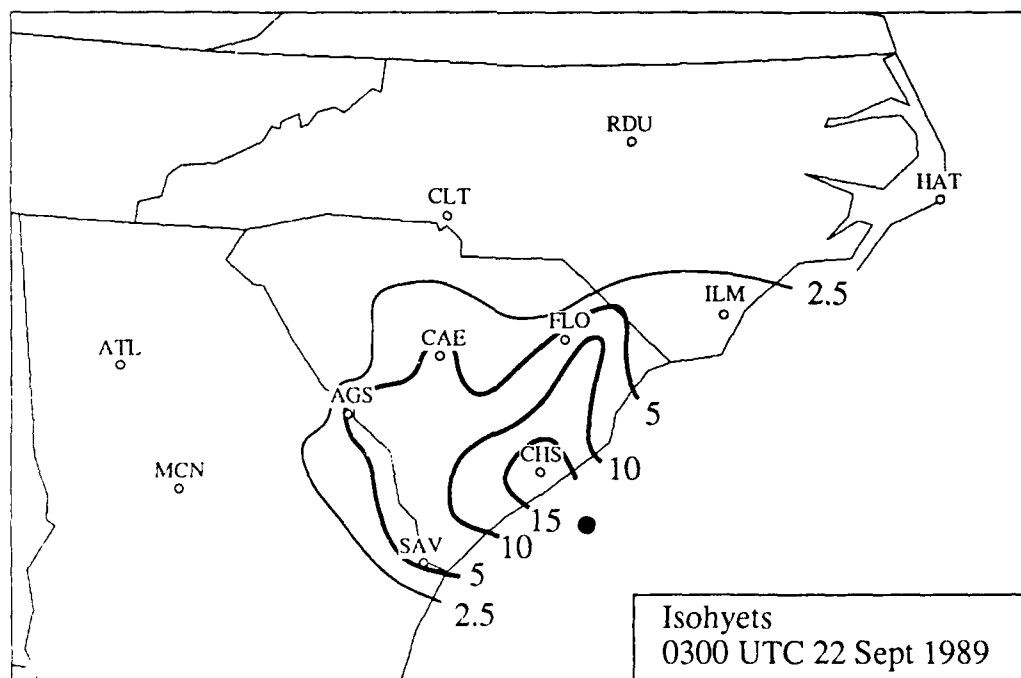
8. d) Analysis of the hourly precipitation data (mm) from 0201 - 0300 UTC
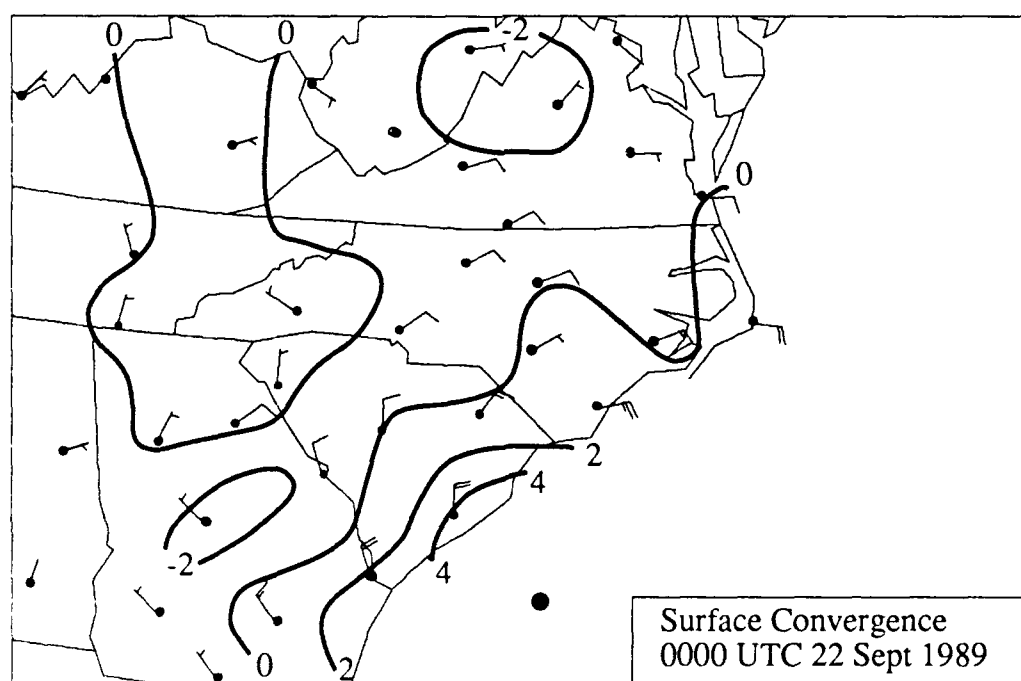on 22 September 1989. Large black dot represents Hugo's eye.

observed. An area of precipitation > 15 mm (Fig. 8d) surrounds Charleston, South Carolina in association with a more pronounced eyewall return. The area of rainfall > 5 mm has reached the central part of the state.

An equivalent potential temperature minima (< 336 K) is analyzed in the SBC at 0600 UTC (Fig. 9a), while equivalent potential temperatures increased from the SBC to the eyewall. This occurred because the SBC acted as a barrier to inward flowing air. Downward mixing in the SBC lowered the equivalent potential temperature of air flowing toward the storm center beneath the SBC. Willoughby *et al.* (1984) documented this fact for a number of storms. A surface low of 956 mb is analyzed near Columbia, South Carolina, and the area of pressures > 1016 mb recedes into central Virginia. The area of strong convergence (> 8×10^{-5} s^{-1}) around Hugo's vortex continues throughout the period (Fig. 9-11b), but shifts from the left of Hugo's track at 0600 UTC to a position ahead of Hugo by 1200 UTC. The patterns of convergence (Fig. 9b) and moderate to heavy precipitation rates (Fig. 9d) are clearly related.

By 0530 UTC (Fig. 9c), Hugo still sustained an open eye in radar reflectivity over South Carolina, with broad VIP level-2 reflectivity encircling two-thirds of the eye. The SBC over Georgia has the largest area of moderate returns with a line of embedded VIP level-3 returns. A large echo free region is observed between the eyewall and SBC which implies that strong subsidence and surface divergence are occurring there. This supports Willoughby *et al.*'s idea that the SBC acts as a barrier to inward flowing air. A precipitation maxima > 20 mm (Fig. 9d) is analyzed in the SBC. There is a definite bias in the precipitation pattern to the left of the vortex center.

The equivalent potential temperature minimum in the SBC decreased by 0900 UTC (Fig. 10a), and a strong equivalent potential temperature gradient continued across the Carolinas. Filling of the surface low to 968 mb has occurred primarily because
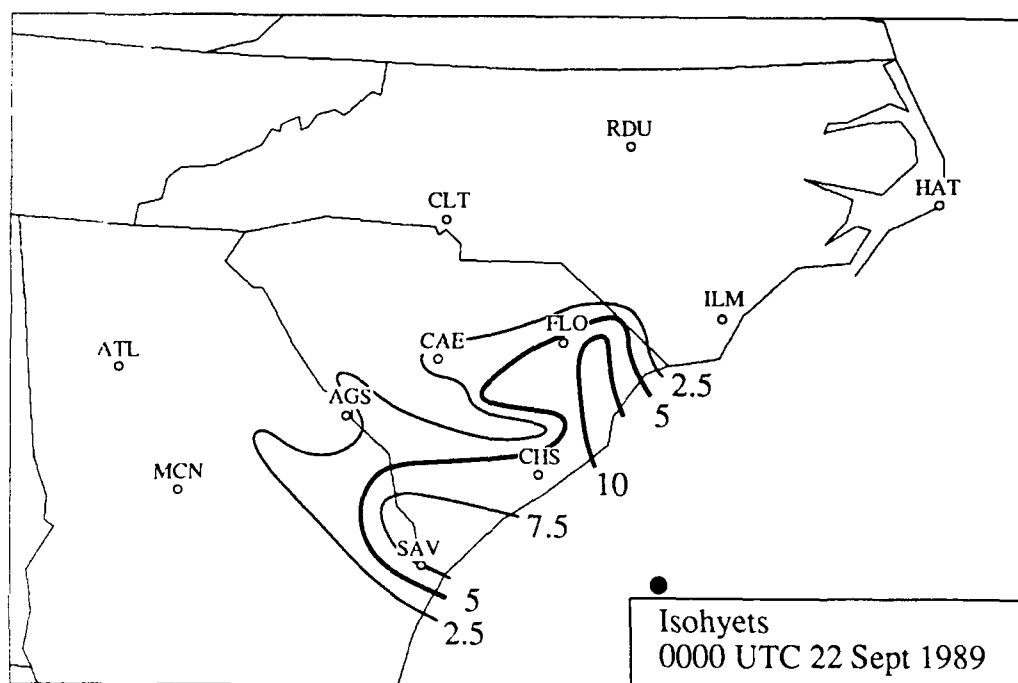
9. a) Surface analysis with sea level pressure (mb) (thick lines) and equivalent potential temperature (K) (thin lines) at 0600 UTC on 22 September 1989. Note that isobars are analyzed at 16 mb increments near the eye.
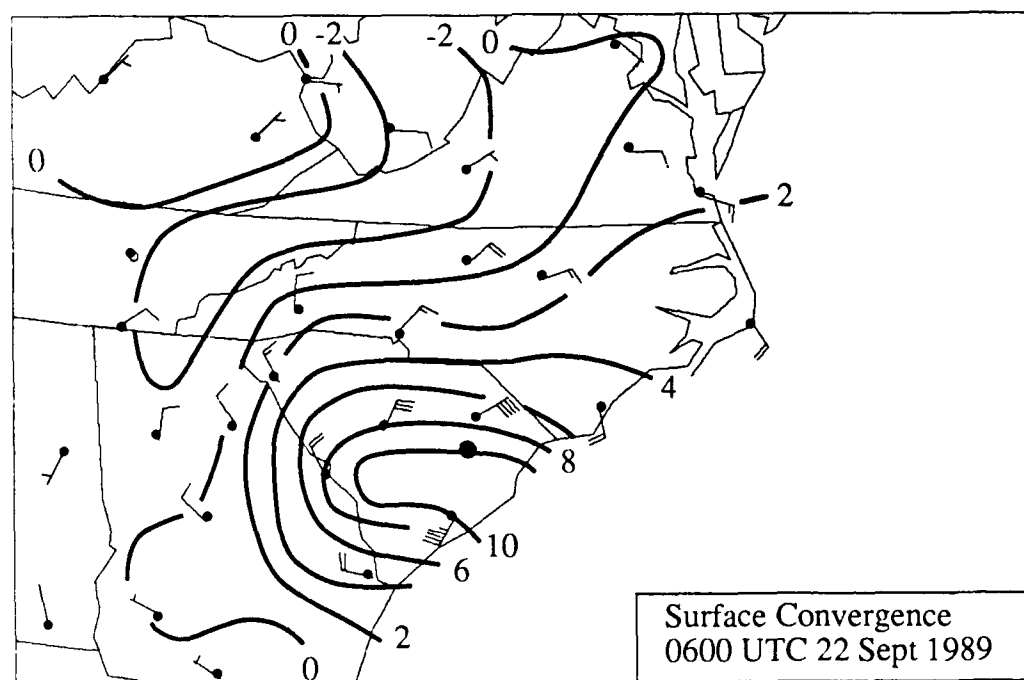
9. b) Surface analysis with wind convergence (10^{-5} s^{-1}) at 0600 UTC on 22 September 1989. Large black dot represents Hugo's eye.
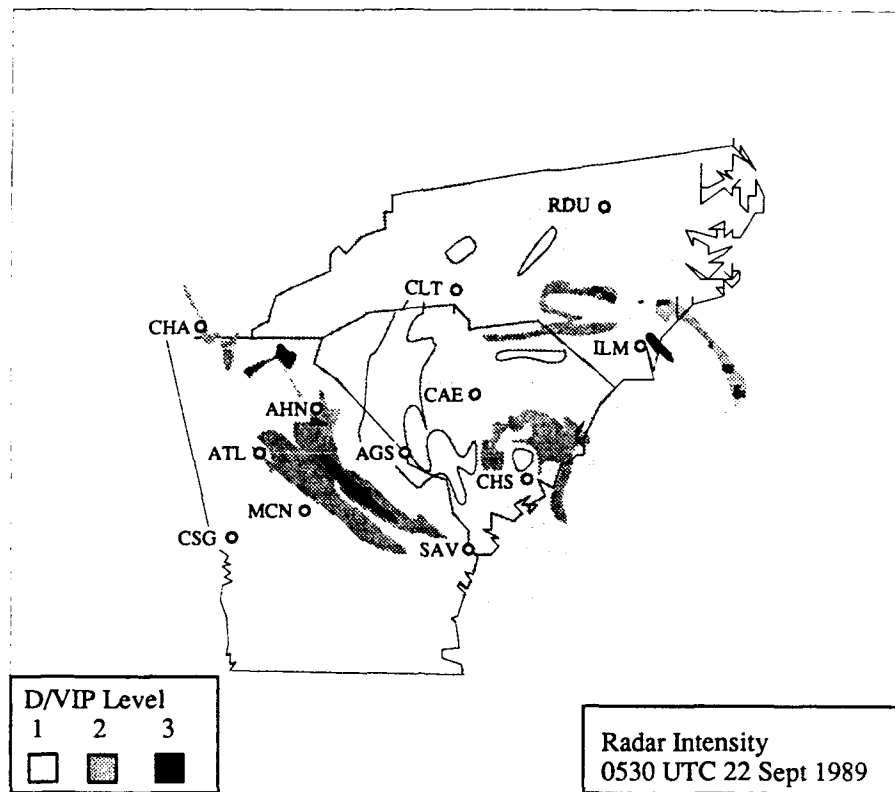
9. c) Composite radar summary with D/VIP levels shaded at 0530 UTC on
22 September 1989.
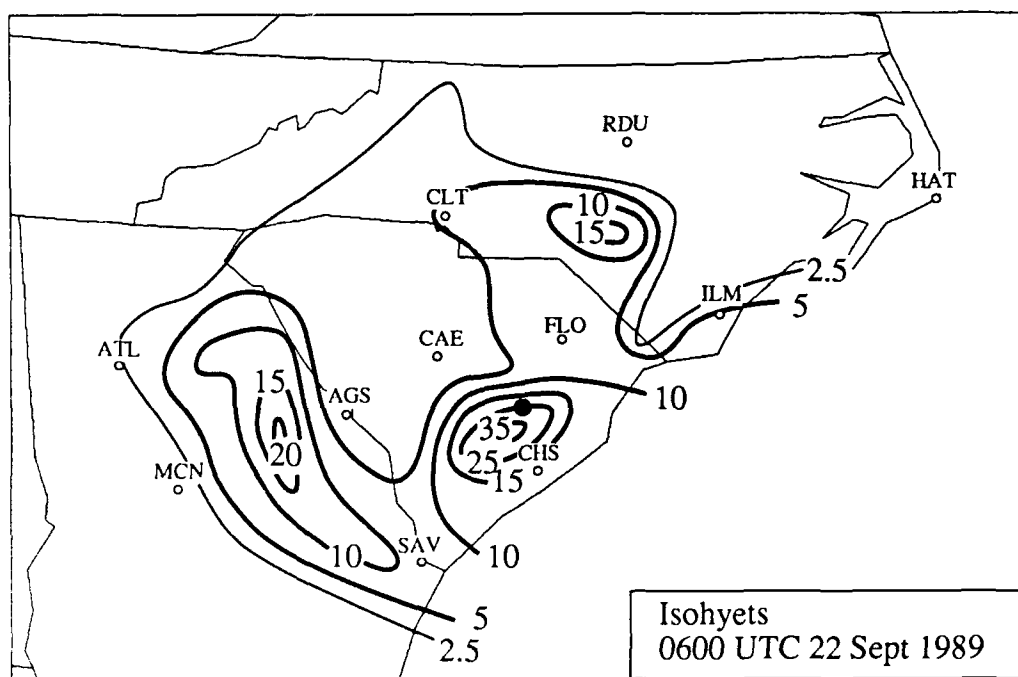
9. d) Analysis of the hourly precipitation data (mm) from 0501 - 0600 UTC
on 22 September 1989. Large black dot represents Hugo's eye.
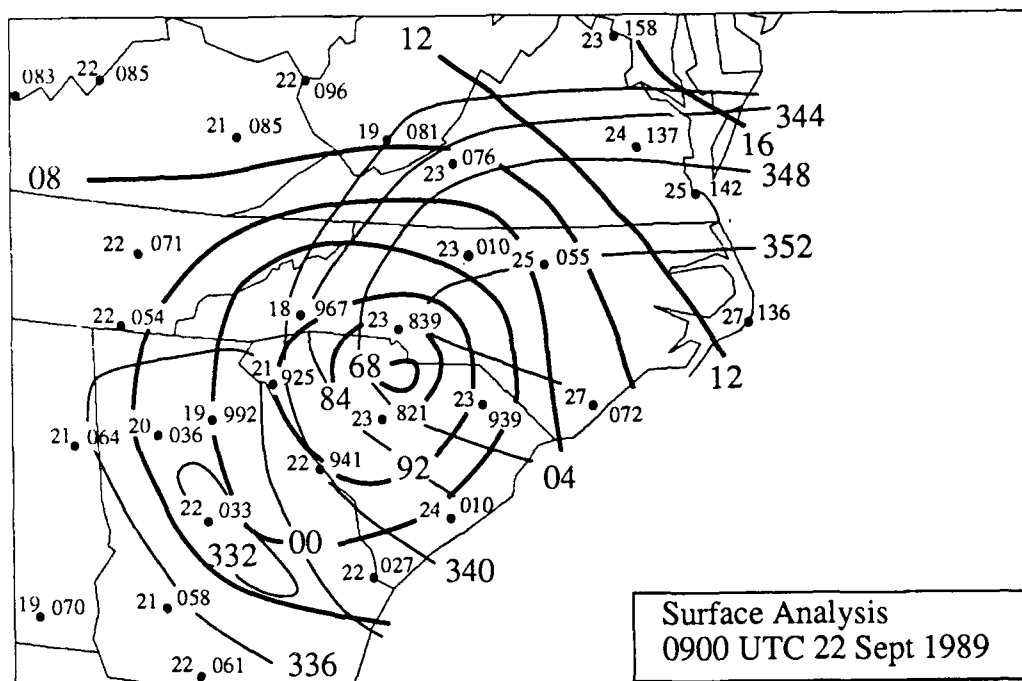
10. a) Surface analysis with sea level pressure (mb) (thick lines) and equivalent potential temperature (K) (thin lines) at 0900 UTC on 22 September 1989. Note that isobars are analyzed at 16 mb increments near the eye.
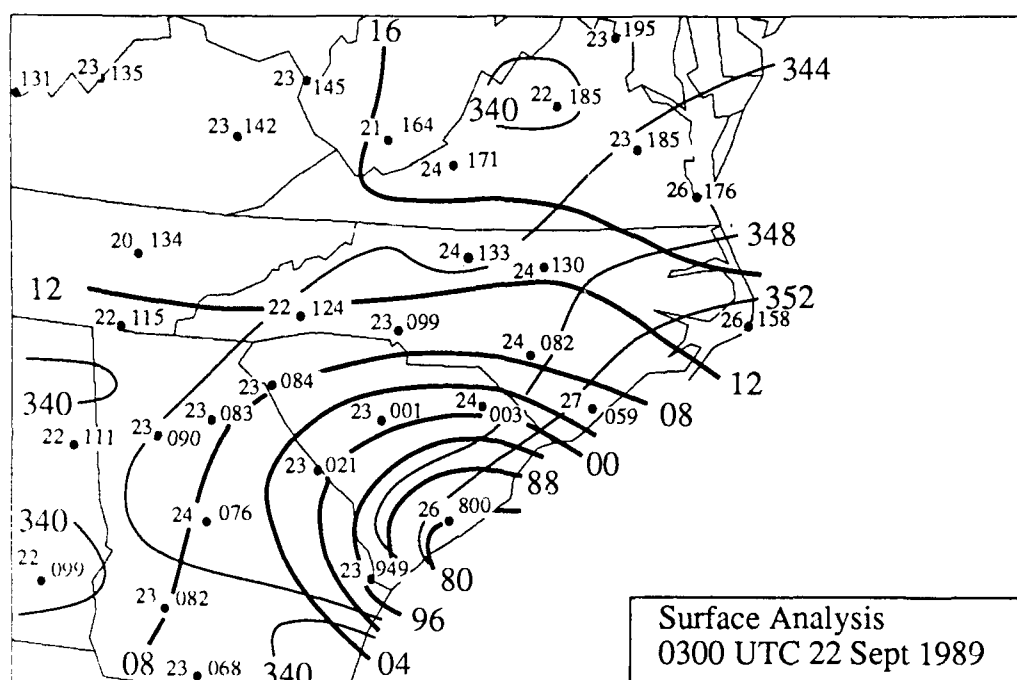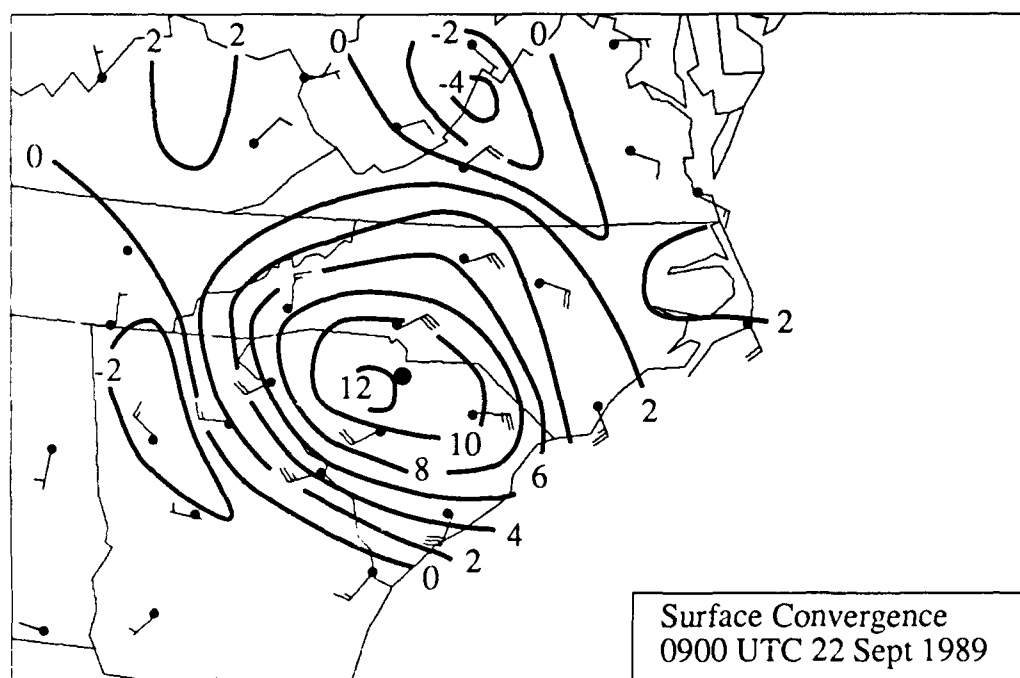

10. b) Surface analysis with wind convergence (10^{-5} s^{-1}) at 0900 UTC on 22 September 1989. Large black dot represents Hugo's eye.
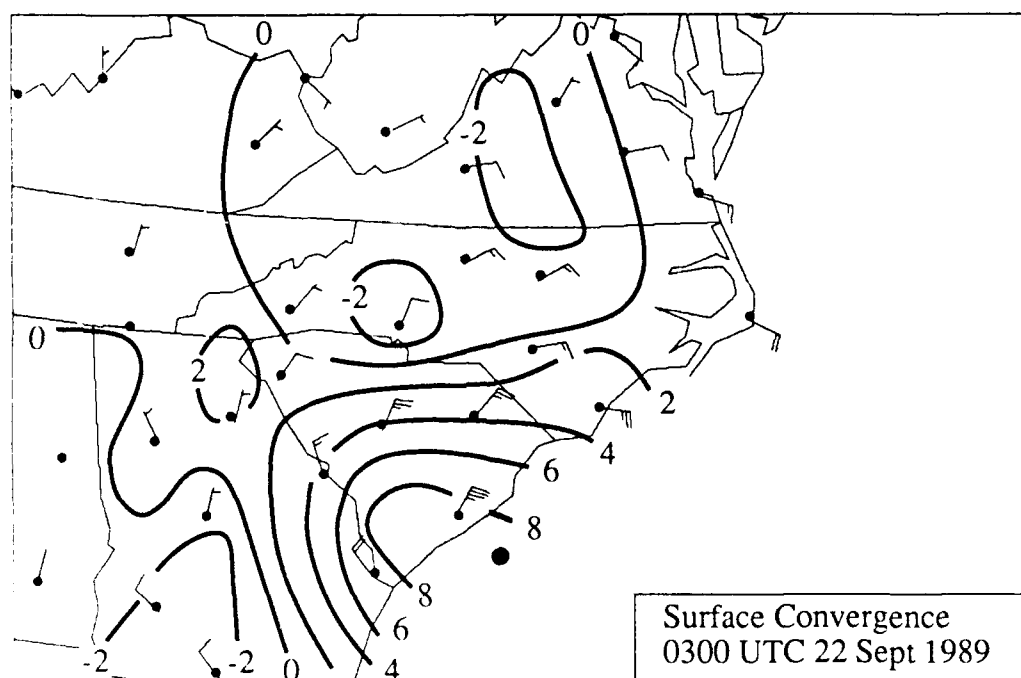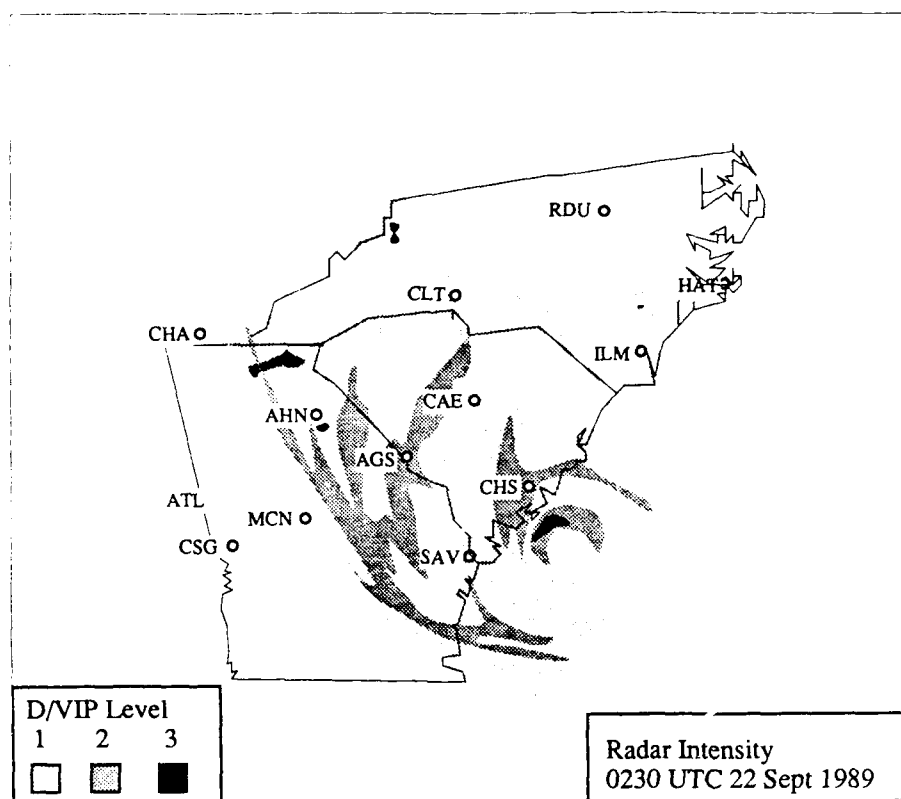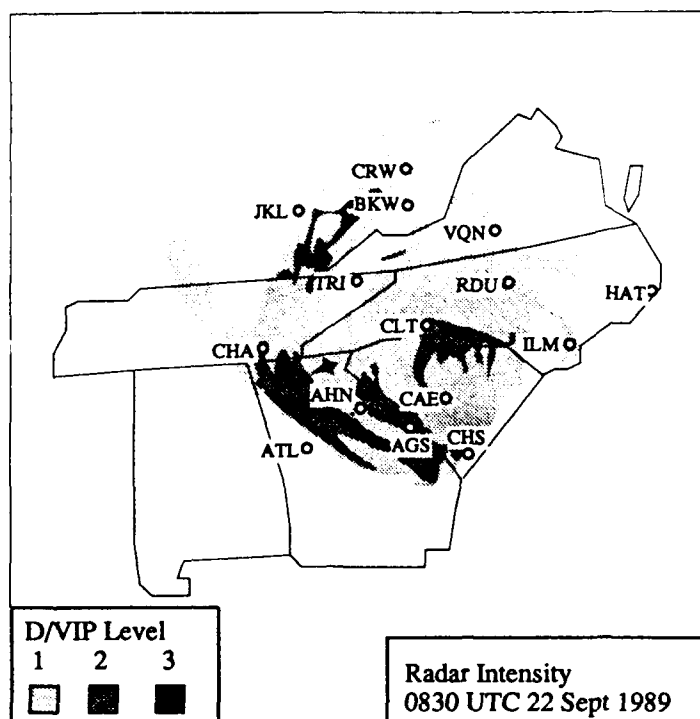
10. c) Composite radar summary with D/VIP levels shaded at 0830 UTC on 22 September 1989.
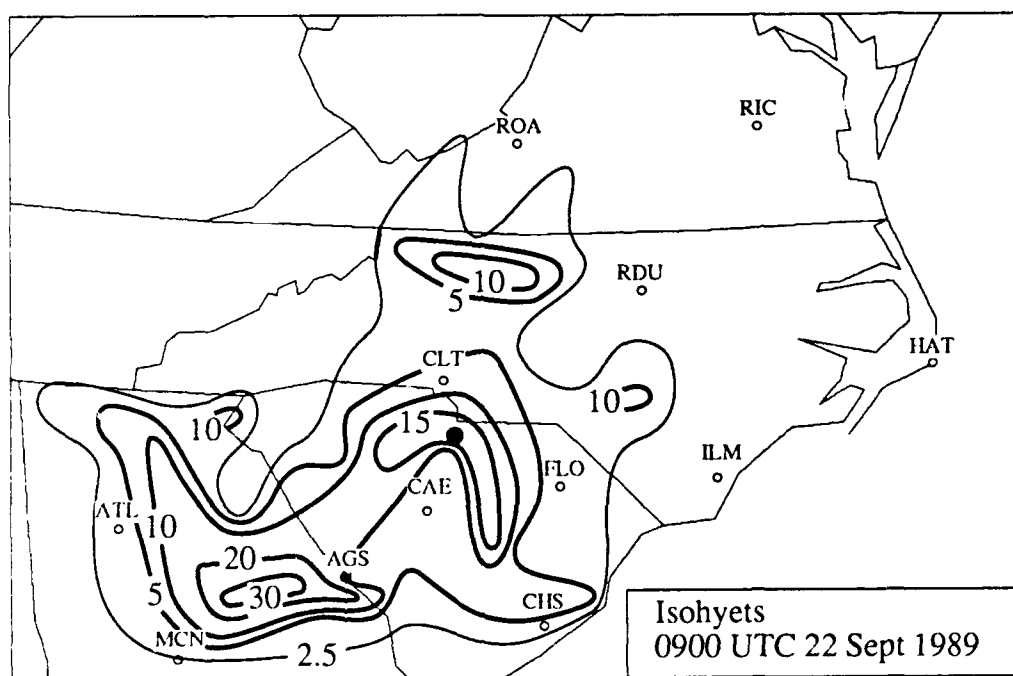
10. d) Analysis of the hourly precipitation data (mm) from 0801 - 0900 UTC on 22 September 1989. Large black dot represents Hugo's eye.

Hugo lost its oceanic latent heat source (Miller, 1963, 1964). By 0830 UTC there is no longer a well-defined eye in radar reflectivity (Fig. 10c) and a weak spiral band has rotated from Virginia into West Virginia. The SBC maintained its position and size with a line of strong returns still present even though surface divergence is observed (Fig. 10b). The pronounced SBC radar signature and longitudinal propagation combine to give rainfall amounts in excess of 30 mm.

There is no pronounced change in the equivalent potential temperature pattern at 1200 UTC (Fig. 11a). Hugo's vortex (near Hickory, North Carolina) continues to fill, but strong convergence still surrounds the center (Fig. 11b). The area of weak reflectivity returns is still large at 1130 UTC (Fig. 11c), but VIP level-2 reflectivity areas are diminishing in size. VIP level-3 returns are isolated to extreme northeast Georgia. The SBC is starting to deteriorate in size and intensity and precipitation rates have diminished to 15 mm h^{-1} or less (Fig. 11d). An area of rainfall > 20 mm, analyzed north of Hugo's vortex, is positively related to radar reflectivity and surface wind convergence.

The above discussion documents predominate precipitation features of Hurricane Hugo, in particular the SBC to the left of Hugo's track maintained its relative size and shape throughout the observation period. As Hugo moved northwestward, the SBC moved northwestward through Georgia along its own length. The stations under this feature experienced prolonged heavy rainfall rates. Amounts of hourly precipitation (> 20 mm) fell within the SBC between 0500 UTC and 1000 UTC. The SBC also acted as a barrier to inward flowing air with convergence occurring along the rainband, but divergence between the SBC and the eyewall. At 0530 UTC and 1130 UTC echo-free regions were observed between the SBC and eyewall. However, these characteristics
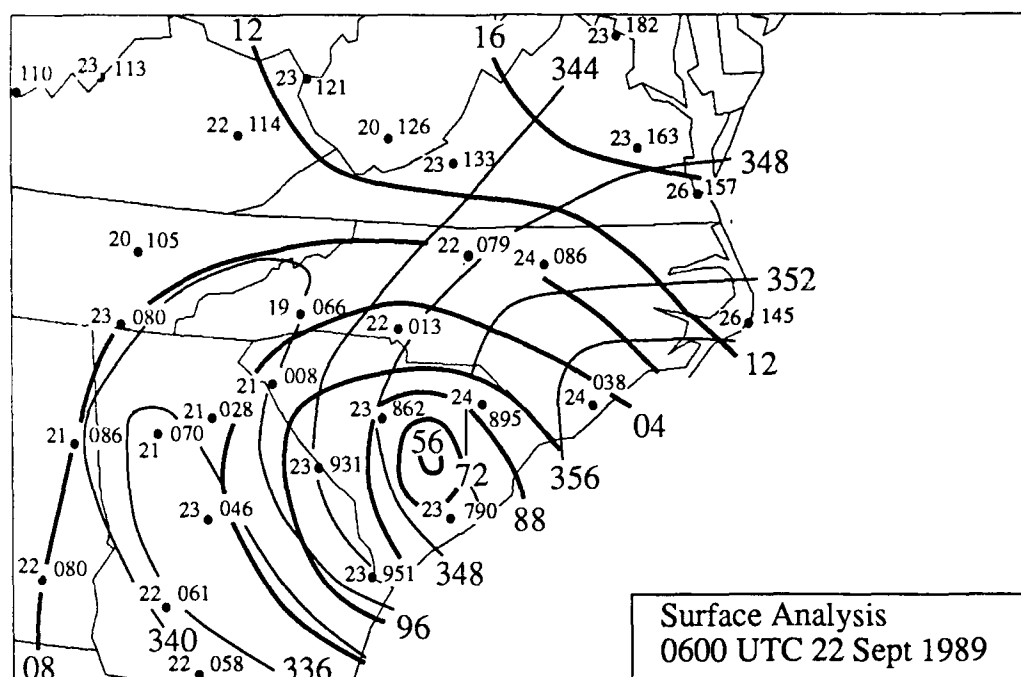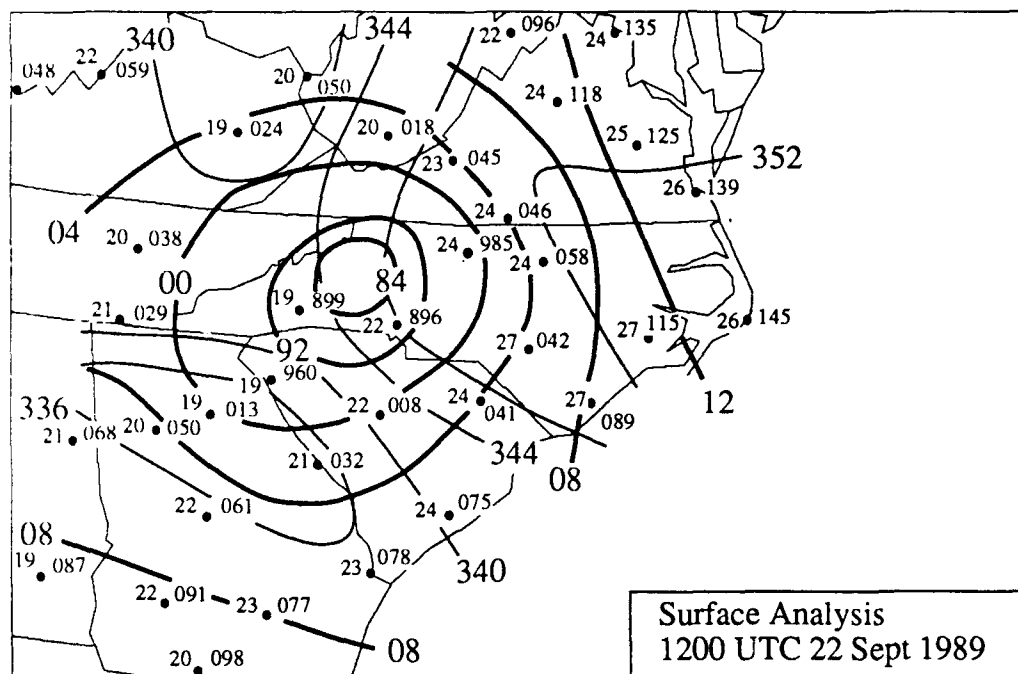
11. a) Surface analysis with sea level pressure (mb) (thick lines) and equivalent potential temperature (K) (thin lines) at 1200 UTC on 22 September 1989. Note that isobars are analyzed at 8 mb increments near the eye.
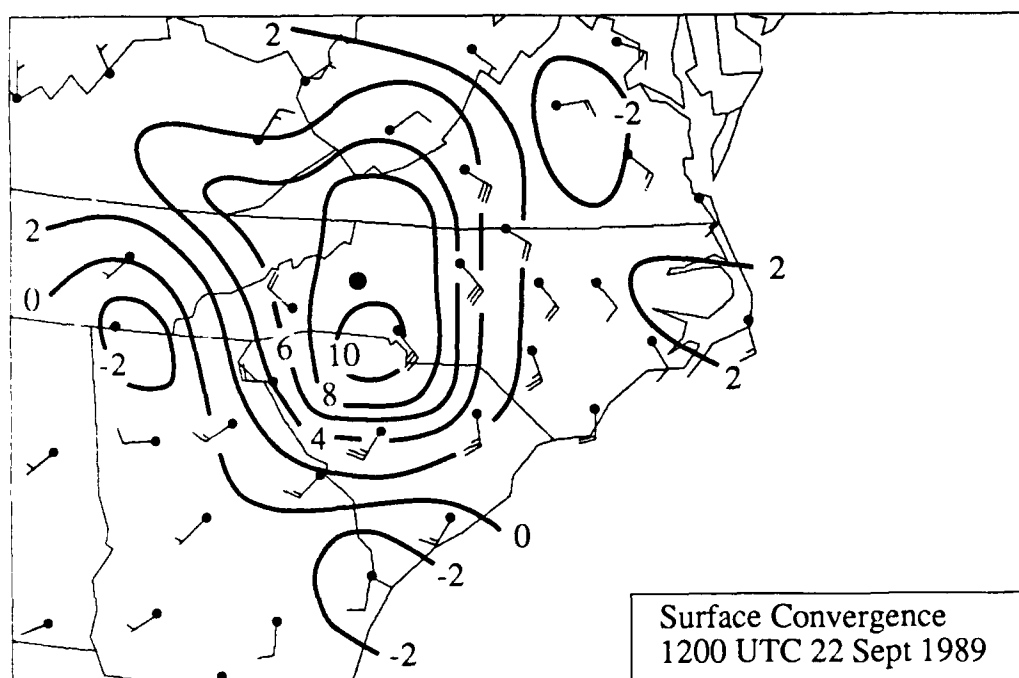
11. b) Surface analysis with wind convergence (10^{-5} s^{-1}) at 1200 UTC on 22 September 1989. Large black dot represents Hugo's eye.
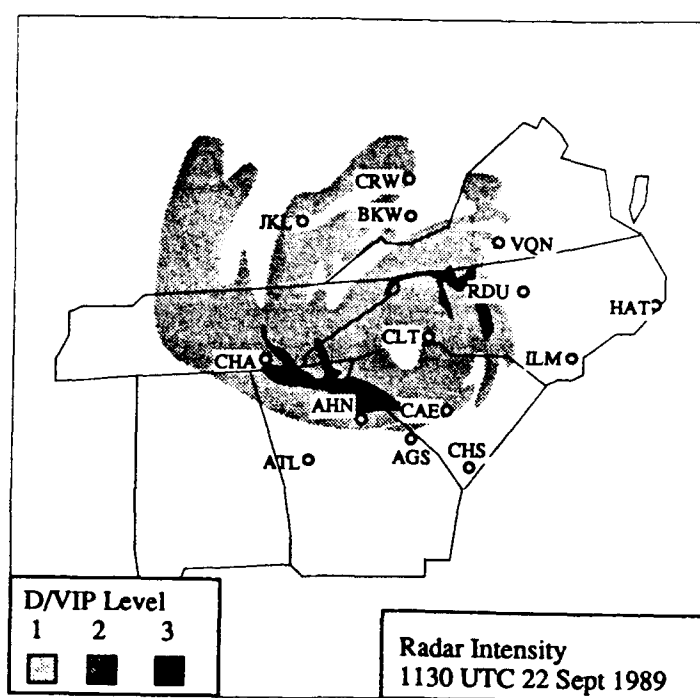
11. c) Composite radar summary with D/VIP levels shaded at
1130 UTC on 22 September 1989.
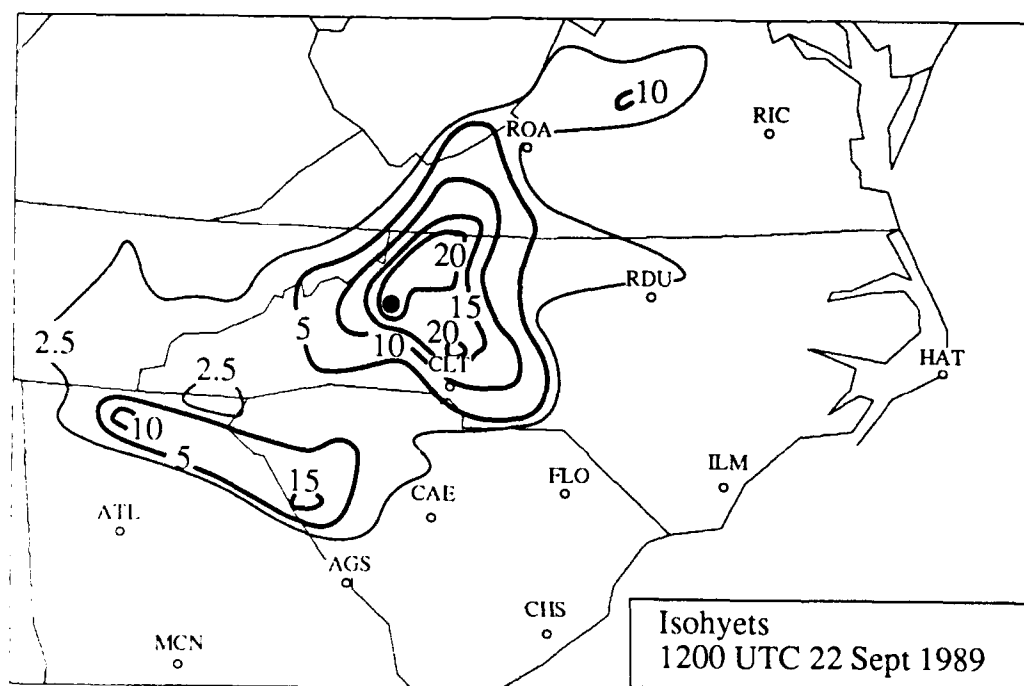
11. d) Analysis of the hourly precipitation data (mm) from 1101 - 1200
UTC on 22 September 1989. Large black dot represents Hugo's eye.

are not identified in the surface wind convergence fields because of inadequate surface station density.

Storm-total precipitation (Fig. 12) for the 19-h period (21 September at 1900 UTC to 22 September at 1300 UTC) indicates that the maximum rainfall (area > 125 mm) occurred near the point of landfall. Three areas of rainfall > 75 mm occur inland; the area over central Georgia is caused by the SBC, and the other two precipitation maxima occur just to the right of Hugo's track in North Carolina. A tongue of precipitation > 50 mm stretching through North Carolina lies just to the east of Hugo's track. However, there was significantly more precipitation and a larger area of rainfall to the left of Hugo's track for the first several hours after landfall.

Hugo's radar reflectivity pattern is very similar to that of Hurricane Frederic after landfall (Parrish et al.,1982). Both possess a strong northern eyewall echo return, northward vortex movement, and a strong convective band west of and moving with the vortex. Frederic's western band and Hugo's SBC both have VIP level-3 reflectivity returns. In both cyclones, the rain totals generally decrease inland from the coast and the maximum rainfall both along the coast and inland is to the left of the vortex path.

The HPD from Hurricane Hugo does not compare favorably with Tuleya *et al.*'s (1984) landfall computer model simulation. In this experiment, slightly more rainfall occurred to the right of the storm track during landfall, but Hugo had notably more precipitation to the left of the storm track (Fig. 10c), due to the SBC.

Two hours after landfall, the model results showed that heavy precipitation > 28.8 mm h^{-1} decreased as the storm decayed. The area of heavy (VIP level-3) rainfall associated with Hugo maintained its size two hours after landfall, but was deteriorating five hours after landfall. The area of weak precipitation started to diminish ~ 13-h after
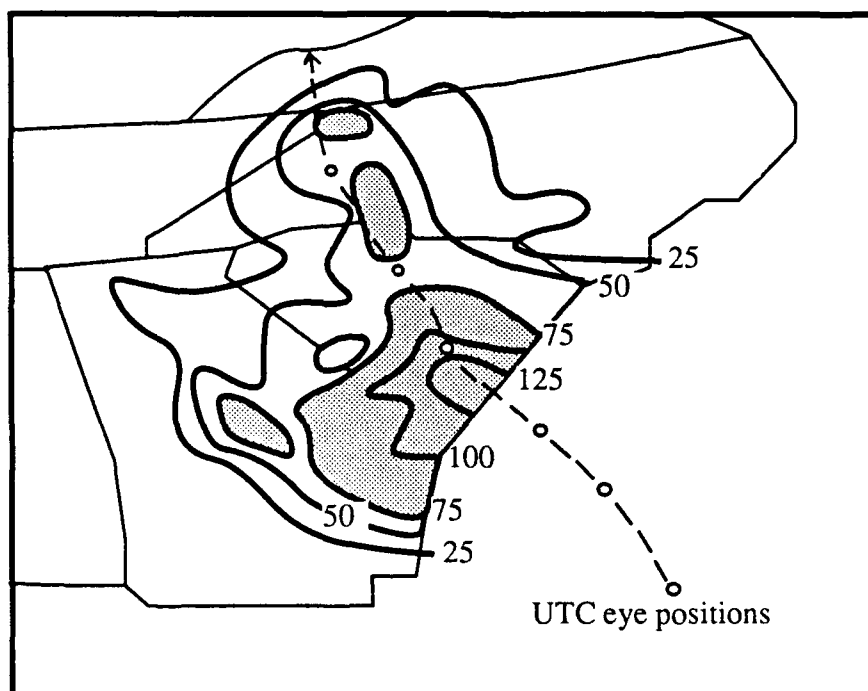
12. Storm-total precipitation (mm) for the 19-h period from
21 September 1989 at 1900 UTC to 22 September at 1300
UTC. Light shading represents rainfall > 50 mm and dark
shading represents rainfall > 75 mm. The eye positions
are in 3-h increments starting at 2100 UTC.

landfall for Tuleya *et al.*'s experiment, but in Hugo the area > 2.5 mm showed no signs of diminishing even 13 hours after landfall.

3. MULTIPLE LINEAR REGRESSION EQUATION

In this chapter, a multiple linear regression model was constructed to predict hourly precipitation for Hugo over the southeastern US. The dependent variable was hourly precipitation data (HPD); while the uncontrolled independent variables examined were distance to eyewall (DEW), wind direction (WD), slope number (SN), wind speed (WS), and wind convergence (CON). The dependence of precipitation rate on position relative to the storm center and direction of movement is accounted for by DEW (distance) and WD (implicit azimuth angle), respectively.

Slope number (SN) is introduced in order to include orographic effects as Hugo approached the Appalachian Mountains. SN is defined by:

$N = \tan(\text{slope angle}) \times (\text{wind speed}) \times [\cos(\text{slope direction} - \text{wind direction})].$

The tan(slope angle) term represents the average terrain incline angle 25 km on both sides of the gridpoint from the coast to the mountains. The wind speed times cos(slope direction - wind direction) term is the component of the wind normal to the terrain contours. SN is thus directly proportional to the up-slope vertical velocity. CON represents regions of ascending motion and can be expected to have some association with precipitation areas.

In this case, the model was

$$Y(\text{obs}) = B_0 + B_1\text{DEW} + B_2\text{WD} + B_3\text{SN} + B_4\text{WS} + B_5\text{CON}$$

and the estimated response was obtained from the sample regression equation

$$y(\text{obs}) = b_0 + b_1\text{DEW} + b_2\text{WD} + b_3\text{SN} + b_4\text{WS} + b_5\text{CON} .$$

By using the observed values of the dependent and independent variables, the regression coefficients B_i could be estimated from b_i and the sample data using the method of least squares (Walpole and Myers, 1989).

The same data set and 3-h time increments described in Chapter 2 provided input to the regression equation. Precipitation data were hourly (ie 2001 -2100 UTC), but all the independent variables were instantaneous values. Gridpoint values were determined using the single pass Barnes scheme mentioned above. Figure 13 shows the gridpoint domain. The residuals for a regression of HPD gave a pattern that indicated increasing variance with increasing level of HPD. This feature violates the assumptions for the ordinary regression model and a transformation was considered to reduce the heteroscadasity of the data. A log transformation of HPD was found to induce nearly constant variability across different levels of this variable. HPD was only examined when precipitation was occurring. Table 2 summarizes the results for the full model. The "F Value" is the model sum of squares divided by the model mean square. The "F Value" and "Prob>F" gives the test statistic and p-value associated with a test of the hypothesis that the model explains a significant portion of the variation in the data. A p-value of 0.0001 indicates that the model explains a significant portion of the variation in the data (ie significant model). "Root MSE" is the square root of the mean square for error. This quantity gives an estimate of the standard deviation. "Dep Mean" gives the overall average for log[HPD]. "R^2" is the model sum of squares divided by the total sum of squares. It indicates how much of the variability of the dependent variable is explained by the regression equation. "R^2" can range from 0 to 1; the closer it is to 1, the better your model is at accounting for variation in the data.
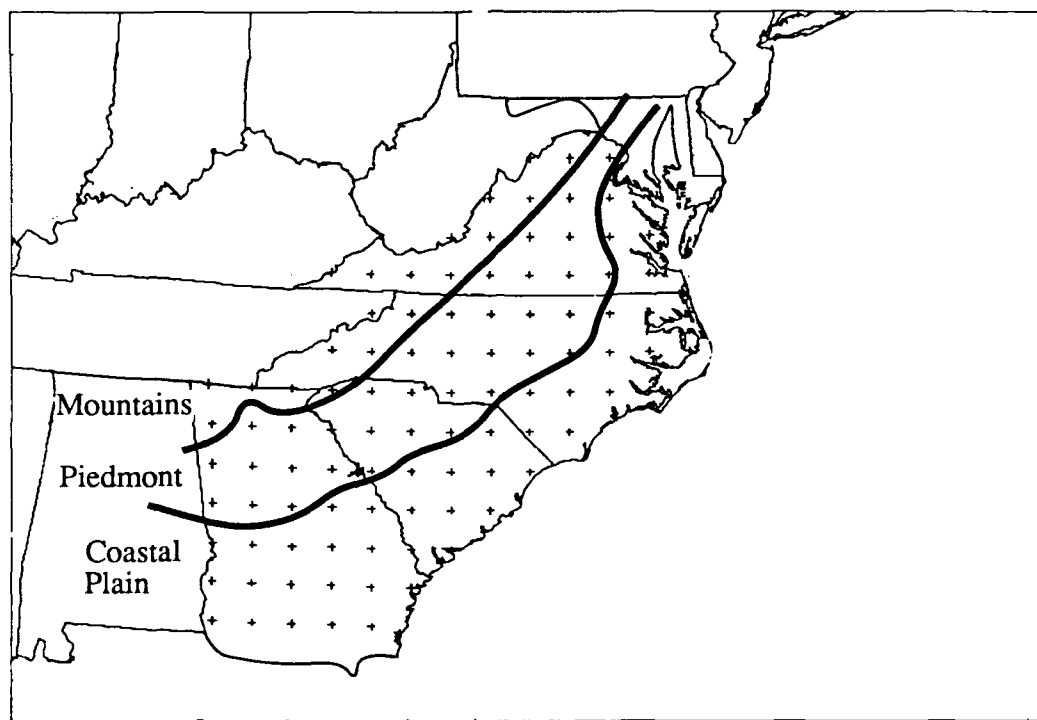
13. Three geographic regions the observation points were seperated into. There are 45 observation points over the Coastal Plain, 35 points over the Piedmont, and 16 points over the Appalachian Mountains.

Table 2 Full Model ANOVA. Summary of statistics from regression estimation of log[HPD]. There were 164 observations.

ANALYSIS OF VARIANCE

SOURCE	F VALUE	PROB>F	Root MSE	R^2	Dep Mean
Model	18.665	0.0001	0.65	0.37	1.36

PARAMETER ESTIMATES

VARIABLE	PARAMETER ESTIMATE	STANDARD ERROR	T FOR Ho: PARAMETER=0	PROB>|T|
Intercept	1.882259	0.290241	6.485	0.0001
DEW	0.003950	0.000814	4.852	0.0001
WD	0.000836	0.000441	1.895	0.0599
SN	0.000023	0.000014	- 1.681	0.0948
WS	0.002918	0.004229	0.690	0.4912
CON	0.009445	0.015581	0.606	0.5452

The "Parameter Estimate" is the variable coefficient for the regression equation. The "Standard Error" measures how much the parameter estimates would vary from one collection of data to the next, and can be used to construct confidence intervals about the parameter estimates. "T for Ho: Parameter=0" gives t-values ("students-t test") for testing the null hypothesis that the parameter equals 0, and these t-values are equal to the parameter estimates divided by their standard errors. "Prob> |T|" gives the p-value for the t-value. A p-value < 0.05 indicates that the slope is not zero at the 95% level of confidence. In other words, the variable is significant.

This equation explains over 37% of the variability of log precipitation for Hugo when precipitation is occurring. The intercept and DEW are significant variables; WD is of questionable significance; while SN, WS, and CON are not significant variables for predicting HPD for Hugo. These results are appropriate for the entire geographic region.

This data set was next separated into three geographic regions (Fig. 13) for further analysis; the Coastal Plain, Piedmont, and Appalachian Mountains. Gridpoints

in each region were combined to produce the respecting regression equations. Table 3 summarizes results for the three regions. 41% of the variability in log HPD was accounted for by the model over the Coastal Plain, 29% over the Piedmont, and 62% over the Appalachians. The equation was more effective at the mountains in part because of the small sample size (21 observations). The intercept and distance to the eyewall (DEW) were again the two most important variables for all geographic regions, but the wind direction became less significant in the regions than it was in the full model.

Wind speed (WS) was more important over the Coastal Plain than the other regions. This makes sense because a tropical storms winds are better organized at landfall than further inland, and the strongest surface winds are in the eyewall where the heaviest precipitation is occurring. 500 km north or south of the eyewall along the coast the winds are lighter and no rainfall is occurring.

Table 3a Region 1 ANOVA. Summary of statistics from regression estimation of log[HPD] for Coastal Plain. There were 72 observations.

ANALYSIS OF VARIANCE

SOURCE	F VALUE	PROB>F	Root MSE	R^2	Dep Mean
Model	9.267	0.0001	0.63	0.41	1.52

PARAMETER ESTIMATES

VARIABLE	PARAMETER ESTIMATE	STANDARD ERROR	T FOR HO: PARAMETER=0	PROB>ITI
Intercept	1.904737	0.401594	4.743	0.0001
DEW	- 0.004243	0.001389	- 3.056	0.0032
WS	0.008118	0.006177	1.314	0.1933
WD	0.000446	0.000609	0.732	0.4666
SN	0.000036	0.000064	0.563	0.5751
CON	0.010352	0.022377	0.463	0.6452

Table 3b Region 2 ANOVA. Summary of statistics from regression estimation of log[HPD] for Piedmont. There were 71 observations.

ANALYSIS OF VARIANCE

SOURCE	F VALUE	PROB>F	Root MSE	R^2	Dep Mean
Model	5.204	0.0005	0.69	0.29	1.24

PARAMETER ESTIMATES

VARIABLE	PARAMETER ESTIMATE	STANDARD ERROR	T FOR HO: PARAMETER=0	PROB>ITI
Intercept	1.726880	0.549915	3.140	0.0025
DEW	- 0.003328	0.001382	- 2.408	0.0189
WD	0.001502	0.000866	1.733	0.0878
SN	- 0.000050	0.000038	- 1.320	0.1914
CON	0.010247	0.025774	0.398	0.6923
WS	- 0.002312	0.008097	- 0.286	0.7761

Table 3c Region 3 ANOVA. Summary of statistics from regression estimation of log[HPD] for Appalachian Mountains. There were 21 observations.

ANALYSIS OF VARIANCE

SOURCE	F VALUE	PROB>F	Root MSE	R^2	Dep Mean
Model	4.898	0.0074	0.60	0.62	1.24

PARAMETER ESTIMATES

VARIABLE	PARAMETER ESTIMATE	STANDARD ERROR	T FOR HO: PARAMETER=0	PROB>ITI
Intercept	2.577750	1.100681	2.342	0.0334
DEW	- 0.005283	0.002651	- 1.993	0.0648
SN	- 0.000022	0.000015	- 1.443	0.1695
WS	- 0.007085	0.016019	- 0.442	0.6646
CON	0.026029	0.069358	0.375	0.7127
WD	0.000264	0.001360	0.194	0.8487

Wind direction (WD) was more important over the Piedmont than the other regions because the wind directions were still fairly organized as Hugo passed through this region. Therefore, heavy precipitation in the SBC quadrant was identified. Slope number (SN) increased in importance from the coast to the mountains as a larger slope in the topography was encountered. DEW decreased in regional importance from the coast since Hugo became less organized as it moved inland. Surface wind convergence (CON) was insignificant in all regions, reflecting the lack of data resolution.

4. SUMMARY AND CONCLUSIONS

Operational surface observations from the National Weather Service and special observations from power plants were used to construct the precipitation distribution and kinematic patterns of Hurricane Hugo over land. One objective of this research was to examine the hourly rainfall distribution, primarily in the stationary band complex (SBC) and eyewall, then compare the precipitation distribution with composite radar reflectivity fields. Another objective was to investigate the inland surface interactions of kinematic fields within the eyewall and SBC. The final objective was to develop a statistical equation that predicts Hugo's hourly rainfall over land.

The period of this study is from 1900 UTC on 21 September 1989 until 1300 UTC on 22 September 1989. Organized convection from Hugo occurs overland at the beginning of this 19-h period, and Hugo's vortex is over the Appalachian Mountains by the end.

Based on the research presented in this paper for Hugo, the following conclusions are drawn:

1) An stationary band complex (SBC) is identified on composite radar data to the left of the eye.

2) Heavy amounts of hourly precipitation (> 30 mm at 0900 UTC) were observed within the SBC between 0500 UTC and 1000 UTC.

3) More precipitation fell to the left of the vortex for 7 hours after Hugo's eye made landfall, due to the SBC. The storm-total rainfall also indicates more precipitation and and a larger area of rainfall to the left of the storms track, until Hugo's eyewall moved into central North Carolina.

4) An area of strong convergence > 8 x 10^{-5} s^{-1} observed around the eye shifts from the left of Hugo at 0600 UTC to just ahead of Hugo by 1200 UTC. Moderate precipitation returns are associated with this area of strong convergence.

5) There was a positive correlation between the SBC and equivalent potential temperature minima for most of the period of this study, due to downward mixing below the SBC.

6) A multiple linear regression equation was constructed that predicted over 37% of the variability of hourly precipitation for Hugo when rainfall was occurring.

7) The distance to the eye wall (DEW) was the only significant physical variable in the regression equation.

8) When the data were separated into geographic regions, the distance to the eye wall (DEW) remained the only significant physical variable in the regression equation. The distance to the eye wall (DEW) decreased in significance away from the coast. Terrain slope was not an important predictor of hourly precipitation for Hugo, but it's contribution increased toward the Appalachian Mountains. Wind speed (WS) was most important over the Coastal Plain, wind direction (WD) was most significant over the Piedmont, and convergence (CON) was insignificant in all regions.

5. APPENDIX

The following pages list the values used in the regression equation. There are 164 observations (OBS) at 3-h increments from 21 September 1989 at 2100 UTC (T = 21) until 22 September at 1200 UTC (T = 12). The three categories are the Coastal Plain (CAT = 1), Piedmont (CAT = 2), and Appalachian Mountains (CAT = 3). The other variables are Hourly Precipitation Data (HPD) (mm), wind direction (WD) (m s^{-1}), surface wind convergence (CON) (10^{-5} s^{-1}), distance to the eyewall (DEW) (km), slope number (SN), and log[HPD] (LHPD).

OBS	T	CAT	HPD	WD	WS	CON	DEW	SN	LHPD
1	21	1	3	355	8.2	-1.60	250	-114.8	1.09861
2	21	1	2	360	7.2	0.20	285	59.7	0.69315
3	21	1	3	360	7.3	2.87	230	- 32.8	1.09861
4	2i	1	2	25	7.9	2.85	295	117.2	0.69315
5	21	1	2	45	9.2	3.86	255	- 14.0	0.69315
6	21	1	3	45	10.5	2.28	320	- 34.9	1.09861
7	00	1	3	340	18.0	1.97	140	308.4	1.09861
8	00	1	3	350	13.3	-2.69	225	-360.4	1.09861
9	00	1	8	355	14.5	1.73	155	498.3	2.07944
10	00	1	9	360	21.8	4.47	100	- 97.9	2.19722
11	00	1	2	360	10.1	-1.08	320	-510.6	0.69315
12	00	1	3	10	12.1	0.82	195	109.6	1.09861
13	00	1	4	15	14.2	2.65	150	-244.0	1.38629
14	00	1	5	30	19.3	4.91	125	194.5	1.60944
15	00	1	4	20	12.1	0.68	210	-200.6	1.38629
16	00	1	8	25	13.7	1.29	195	-313.4	2.07944

17	00	1	5	30	15.4	1.37	205	173.0	1.60944
18	00	1	2	25	11.6	-5.41	260	-130.0	0.69315
19	00	1	2	30	12.0	-3.92	275	-270.5	0.69315
20	00	2	1	30	11.2	-5.90	275	-229.8	0.00000
21	03	1	3	305	46.2	8.78	¡70	-745.4	1.09861
22	03	1	2	315	31.3	10.50	225	1050.5	0.69315
23	03	1	8	325	46.4	11.00	150	315.7	2.07944
24	03	1	14	350	63.2	9.59	80	358.8	2.63906
25	03	1	4	360	29.6	9.45	230	326.7	1.38629
26	03	1	7	15	38.5	9.16	155	360.5	1.94591
27	03	1	10	20	48.5	9.64	100	-201.0	2.30259
28	03	1	11	45	55.0	10.30	50	- 83.8	2.39790
29	03	1	5	25	29.2	3.69	200	-872.4	1.60944
30	03	1	7	25	32.6	5.43	145	1934.1	1.94591
31	03	1	11	45	34.3	7.04	120	-351.9	2.39790
32	03	1	3	80	31.6	7.08	125	276.2	1.09861
33	03	1	2	45	22.5	1.24	180	565.2	0.69315
34	03	1	2	55	20.2	3.06	190	-440.6	0.69315
35	03	1	3	75	18.5	3.96	220	167.2	1.09861
36	03	2	2	15	23.6	-1.49	245	1704.7	0.69315
37	03	2	2	25	24.0	-3.35	205	802.6	0.69315
38	06	1	2	260	32.0	6.94	230	809.1	0.69315
39	06	¡	5	270	43.3	7.38	190	520.8	1.60944
40	06	1	2	310	15.3	1.27	315	29.0	0.69315
41	06	1	6	285	34.3	7.15	245	- 7.7	1.79176
42	06	1	10	280	52.1	9.11	185	-1748.6	2.30259

43	06	1	8	275	64.9	6.89	130	-148.1	2.07944
44	06	1	13	320	72.9	5.33	95	27.6	2.56495
45	06	1	15	335	49.5	10.20	225	-2655.9	2.70805
46	06	1	10	350	69.7	8.65	160	1040.0	2.30259
47	06	1	5	360	78.0	5.92	95	329.5	1.60944
48	06	1	30	15	80.6	5.65	30	-1385.0	3.40120
49	06	1	13	140	76.0	7.53	50	- 796.8	2.56495
50	06	1	3	30	78.4	5.93	95	-7182.2	1.09861
51	06	1	4	35	78.3	5.96	30	-2413.8	1.38629
52	06	1	8	90	69.2	7.52	45	832.5	2.07944
53	06	1	6	130	50.3	9.15	115	283.3	1.79176
54	06	1	7	75	50.8	4.78	100	- 982.9	1.94591
55	06	1	2	105	33.1	7.43	150	- 636.0	0.69315
56	06	1	4	115	23.1	8.16	200	113	1.38629
57	06	1	15	90	19.5	4.35	195	- 807	2.70805
58	06	1	5	105	14.2	2.17	345	- 68	1.60944
59	06	2	3	335	18.3	4.90	300	1534	1.09861
60	06	2	2	5	7.1	1.14	370	- 382	0.69315
61	06	2	5	5	19.0	7.03	300	-2169	1.60944
62	06	2	12	360	48.6	9.33	230	3882	2.48491
63	06	2	2	10	70.1	7.62	160	-5684	0.69315
64	06	2	1	10	17.7	4.96	320	-3434	0.00000
65	06	2	5	5	33.5	5.50	250	-3060	1.60944
66	06	2	2	5	52.6	6.05	190	- 885	0.69315
67	06	2	1	20	65.6	5.27	130	4898	0.00000
68	06	2	5	40	64.9	4.10	95	- 328	1.60944

69	06	2	3	10	30.4	1.90	225	-1091	1.09861
70	06	2	4	15	40.4	2.12	185	1294	1.38629
71	06	2	5	35	40.1	0.97	160	-1132	1.60944
72	06	2	8	70	28.3	1.68	160	-1596	2.07944
73	06	2	3	30	20.4	-1.63	250	- 563	1.09861
74	06	2	2	45	20.2	-4.46	225	- 986	0.69315
75	06	2	2	75	16.3	0.98	230	-1245	0.69315
76	06	2	1	80	14.0	2.11	255	397	0.00000
77	06	3	3	10	22.4	1.06	285	-13550	1.09861
78	06	3	2	20	18.3	-2.08	280	-2514	0.69315
79	06	3	2	40	13.2	-3.77	310	4566	0.69315
80	09	1	2	275	10.5	0.66	295	- 146	0.69315
81	09	1	2	260	17.4	-1.29	245	- 12	0.69315
82	09	1	2	245	22.1	-3.14	210	599	0.69315
83	09	1	28	275	29.0	3.04	200	1307	3.33220
84	09	1	25	250	36.2	0.56	150	- 328	3.21888
85	09	1	4	235	38.1	-1.21	120	378	1.38629
86	09	1	4	220	37.3	-3.21	125	468	1.38629
87	09	1	5	190	32.4	2.50	160	- 251	1.60944
88	09	1	10	200	50.9	6.58	55	-4445	2.30259
89	09	1	15	185	47.6	7.83	70	-3119	2.70805
90	09	1	4	175	38.1	9.62	125	- 582	1.38629
91	09	1	4	160	41.6	13.20	110	584	1.38629
92	09	1	6	130	25.1	7.99	190	326	1.79176
93	09	1	1	130	18.5	3.64	260	260	0.00000
94	09	1	1	105	9.8	1.58	470	337	0.00000

95	09	2	1	310	7.7	1.32	320	- 396	0.00000
96	09	2	10	305	14.6	3.44	255	- 83	2.30259
97	09	2	3	320	9.6	1.46	300	- 202	1.09861
98	09	2	9	330	22.7	5.68	235	172	2.19722
99	09	2	2	330	41.7	8.23	165	222	0.69315
100	09	2	7	275	49.5	7.49	100	-1480	1.94591
101	09	2	5	330	11.9	0.96	295	- 493	1.60944
102	09	2	5	340	28.6	4.39	225	5435	1.60944
103	09	2	1	340	46.5	7.73	150	2077	0.00000
104	09	2	2	330	56.6	9.11	80	2529	0.69315
105	09	2	10	225	59.8	9.90	10	-5398	2.30259
106	09	2	14	180	55.6	12.10	40	-2425	2.63906
107	09	2	3	355	58.3	5.72	115	2830	1.09861
108	09	2	13	340	64.0	8.10	65	1754	2.56495
109	09	2	9	175	59.7	11.50	75	3629	2.19722
110	09	2	3	140	42.3	12.20	130	-1841	1.09861
111	09	2	3	50	62.9	4.89	135	-7096	1.09861
112	09	2	3	95	59.9	8.92	145	-4351	1.09861
113	09	2	3	120	42.4	10.10	175	-2583	1.09861
114	09	2	2	120	24.4	6.17	230	- 530	0.69315
115	09	2	1	125	17.4	2.64	290	- 605	0.00000
116	09	2	10	75	54.8	7.34	205	1318	2.30259
117	09	2	5	90	41.0	9.48	235	-2143	1.60944
118	09	2	3	70	32.6	7.39	300	-6078	1.09861
119	09	2	1	95	20.4	4.91	330	265	0.00000
120	09	2	5	75	15.8	0.17	380	-2291	1.60944

121	09	2	3	95	10.7	0.44	425	70	1.09861
122	09	2	3	85	9.4	-4.11	480	290	1.09861
123	09	3	2	330	7.1	-5.06	365	0	0.69315
124	09	3	5	345	46.7	3.73	175	13817	1.60944
125	09	3	2	5	56.1	2.20	155	6076	0.69315
126	09	3	7	55	55.6	3.54	200	-21953	1.94591
127	09	3	3	65	38.3	3.63	275	1963	1.09861
128	09	3	1	65	39.0	6.04	280	16818	0.00000
129	09	3	1	70	12.3	-3.93	450	- 2891	0.00000
130	12	1	2	205	19.6	6.32	220	- 1011	0.69315
131	12	1	1	190	17.9	5.85	240	- 693	0.00000
132	12	2	5	235	20.6	5.02	220	- 751	1.60944
133	12	2	3	255	11.0	-3.17	280	292	1.09861
134	12	2	6	260	20.6	-1.49	225	- 1307	1.79176
135	12	2	10	255	27.5	5.69	175	- 822	2.30259
136	12	2	7	240	29.5	9.23	150	- 326	1.94591
137	12	2	3	215	27.0	10.00	150	2282	1.09861
138	12	2	3	245	42.8	8.45	85	-2342	1.09861
139	12	2	4	200	40.9	9.91	85	-1693	1.38629
140	12	2	6	180	29.9	8.93	130	42	1.79176
141	12	2	3	165	18.2	4.53	185	- 875	1.09861
142	12	2	18	145	51.7	7.44	30	-4971	2.89037
143	12	2	16	140	39.1	6.75	100	1208	2.77259
144	12	2	5	135	21.6	2.91	160	1732	1.60944
145	12	2	15	110	40.8	6.28	105	-1568	2.70805
146	12	2	3	120	24.2	3.03	170	-1265	1.09861

147	12	2	3	130	16.8	0.24	245	-1045	1.09861
148	12	2	1	145	14.2	0.71	310	785	0.00000
149	12	2	2	110	23.1	3.50	200	1352	0.69315
150	12	2	5	105	17.7	-9.12	300	-4124	1.60944
151	12	2	2	110	13.9	-2.55	355	130	0.69315
152	12	2	1	105	13.4	-2.92	390	-1109	0.00000
153	12	2	1	110	11.0	-6.46	490	- 383	0.00000
154	12	3	2	260	6.4	-2.12	345	0	0.69315
155	12	3	2	255	31.0	2.62	185	-3502	0.69315
156	12	3	3	260	39.2	6.52	125	-7756	1.09861
157	12	3	5	255	50.9	6.36	100	129	1.60944
158	12	3	20	230	53.8	6.64	30	6379	2.99573
159	12	3	21	105	53.7	6.71	45	-19465	3.04452
160	12	3	7	90	44.5	7.59	110	327	1.94591
161	12	3	12	95	32.9	6.73	145	6000	2.48491
162	12	3	3	95	20.5	2.73	245	2744	1.09861
163	12	3	2	90	18.2	1.58	300	5168	0.69315
164	12	3	3	105	12.3	-1.92	440	- 963	1.09861

6. REFERENCES

Bradbury, D. L., 1971: The filling over land of hurricane Camille, August 17-18, 1969. SMRP Res. Pap. No. 96, Dept. Geophys. Sci., University of Chicago, 25 pp.

Case, B. and M. Mayfield, 1990: Annual Summaries: Atlantic hurricane season of 1989. *Mon. Wea. Rev.*, **118**, 1171-1175.

Chow, S., 1971: A study of the wind field in the planetary boundary layer of a moving tropical cyclone. M.S. thesis, Dept. Meteor. Oceanogr., New York University, 59 pp. [NHRL Library, Coral Gables, FL. 33146].

Cline, I. M., 1926: Tropical Cyclones. MacMillan, 301 pp.

Dunn, G. E., and B. I. Miller, 1960: Atlantic Hurricanes. Louisiana State University Press, 377 pp.

Federal Meteorological Handbook No. 7A, 1987: Weather Radar Observations. US Department of Commerce/Defense, 58 pp.

Koteswaram, P., and S. Gasper, 1956: The surface structure of tropical cyclones in the Indian area. *Ind. J. Meteor. Geophys.*, **7**, 339-352.

Miller, B. I., 1958: The three-dimensional wind structure around a tropical cyclone. NHRP Rep. No. 15, U.S. Dept. Commerce, 41 pp. [NOAA/NHRL, 1320 S. Dixie Hwy., Coral Gables, FL. 33146].

_____, 1963: On the filling of tropical cyclones over land. NHRP Rep. No. 66, U.S. Dept. Commerce, 82 pp. [NOAA/NHRL, 1320 Dixie Hwy., Coral Gables, FL. 33146].

_____, 1964: A study of the filling of Hurricane Donna (1960) over land. *Mon. Wea. Rev.*, **92**, 389-406.

Moss, M. S., and R. W. Jones, 1978: A numerical simulation of hurricane landfall. NOAA Tech. Memo, ERL NHEML-3, U.S. Dept. Commerce, 15 pp. [NOAA/NHRL, 1320 S. Dixie Hwy., Coral Gables, FL. 33146].

Myers, V. A., and W. Malkin, 1961: Some properties of hurricane wind fields as deduced from trajectories. NHRP Rep. No. 49, U.S. Dept. Commerce, 45 pp. [NOAA/NHRL, 1320 S. Dixie Hwy., Coral Gables, FL. 33146].

Parrish, J. R., R. W. Burpee, and F. D. Marks, Jr., 1982: Rainfall patterns observed by digitized radar during the landfall of Hurricane Frederick (1979). *Mon. Wea. Rev.*, **110**, 1933-1944.

Powell, M. D., 1982: The transition of the Hurricane Frederick boundary layer wind fields from the open gulf of Mexico to landfall. *Mon. Wea. Rev.*, **110**, 1912-1932.

_____, 1987: Changes in the low-level kinematic and thermodynamic structure of Hurricane Alicia (1983) at landfall. *Mon. Wea. Rev.*, **115**, 75-99.

Sheets, R. C., 1990: The National Hurricane Center-Past, present, and Future. *Wea. and Forecasting*, **5**, 185-232.

Simpson, R. H., A. L. Sugg, G. B. Clark, N. L. Frank, J. R. Hope, P. J. Hebert, R. H. Kraft, and J. M. Pelissier, 1970: The Atlantic hurricane season of 1969. *Mon. Wea. Rev.*, **98**, 293-301.

Tuleya, R. E., M. A. Bender, and Y. Kurihara, 1984: A simulation study of the landfall of tropical cyclones using a movable nested-mesh model. *Mon. Wea. Rev.*, **112**, 124-136.

Walpole, R. E., and R. H. Myers, 1989: Probability and statistics for engineers and scientists. MacMillan Publishing Company, 765 pp.

Willoughby, H. E., F. D. Marks, Jr., and R. J. Feinberg, 1984: Stationary and moving convective bands in hurricanes. *J. Atmos. Sci.*, **41**, 3189-3211.